


RESEARCH

Open Access



An archaeometric contribution to the interpretation of blue-green glass beads from Iron age Central Italy

Oleh Yatsuk^{1*}, Leonie Koch² , Astrik Gorghinian³, Giacomo Fiocco^{4,5}, Patrizia Davit¹, Lorena Carla Giannossa^{6,7}, Annarosa Mangone^{6,7}, Serena Francone⁸, Alessandra Serges⁸, Alessandro Re⁹, Alessandro Lo Giudice⁹, Marco Ferretti¹⁰, Marco Malagodi^{4,5}, Cristiano Iaia¹¹ and Monica Gulmini¹

Abstract

Several types of (mostly) blue-green glass beads from Iron-Age archaeological sites in Central Italy were studied using a range of spectroscopic techniques: portable X-Ray Fluorescence spectrometry, Fibre Optics Reflectance Spectroscopy, Scanning Electron Microscopy coupled with Energy Dispersive X-ray Spectrometry, micro-Raman spectroscopy and Laser Ablation Inductively Coupled Plasma Mass Spectrometry. Complementary information was gathered from each technique and discussed in the frame of the archaeological typology of the objects. The systematic evaluation of the results allowed us to draw some conclusions on the raw materials employed for primary production and to highlight some provenance indicators in the glass. Some of the beads found in the Iron Age (IA) contexts were preliminarily attributed to the Final Bronze Age (FBA) production based on their typology, and the compositional data obtained in this work confirmed that they were low magnesium high potassium (LMHK) glass, typical of FBA in the Italian peninsula. Other beads were assigned to low magnesium glass (LMG) or high magnesium glass (HMG), thus giving further information on the fluxing agents employed in the Early Iron Age (EIA) and beyond. Colour variations among the beads reflected their chemical composition, with different bead typologies coloured in a specific way. In some instances, it was possible to establish different origins for the colouring raw materials. The provenance of the samples was difficult to place, but the chemical evidence suggested a subdivision within the raw glass used to produce the beads: for one set of samples, a local origin of the glass could be hypothesised, whereas several production sites in the Near East were suggested for most of the beads considered in this study. Some preliminary clues for the local working of imported glass were also highlighted for one typological group.

Keywords Archaeological glass, Glass beads, Iron age, Late bronze age, FORS, XRF, LA-ICP-MS

*Correspondence:

Oleh Yatsuk

oleh.yatsuk@unito.it

Full list of author information is available at the end of the article



© The Author(s) 2023. **Open Access** This article is licensed under a Creative Commons Attribution 4.0 International License, which permits use, sharing, adaptation, distribution and reproduction in any medium or format, as long as you give appropriate credit to the original author(s) and the source, provide a link to the Creative Commons licence, and indicate if changes were made. The images or other third party material in this article are included in the article's Creative Commons licence, unless indicated otherwise in a credit line to the material. If material is not included in the article's Creative Commons licence and your intended use is not permitted by statutory regulation or exceeds the permitted use, you will need to obtain permission directly from the copyright holder. To view a copy of this licence, visit <http://creativecommons.org/licenses/by/4.0/>. The Creative Commons Public Domain Dedication waiver (<http://creativecommons.org/publicdomain/zero/1.0/>) applies to the data made available in this article, unless otherwise stated in a credit line to the data.

Introduction

This paper aims at contributing new knowledge on the glass circulating in the Iron Age (IA) through archaeometric data obtained by different analytical techniques from forty glass beads (whole beads or fragments) found in several burial sites in the historical regions called

Etruria and Latium, in present-day Central Italy (Fig. 1).

The samples were selected in order to represent different types of blue-green glass beads from funerary contexts dated to the Early Iron Age (EIA) I, EIA II, Early Orientalizing and Middle Orientalising periods, which means from the 10th–9th to the 7th century BCE, with a prevalence of beads from contexts of the EIA. The beads are presently preserved in two archaeological museums, namely the Museo Nazionale Etrusco di Villa Giulia and the Museo delle Civiltà (both in Rome, Italy).

All the beads were studied thoroughly to identify their typology based on macroscopic evidence, to support the discussion of the archaeometric data for a period that is particularly relevant for archaeological glass studies. Glass-making recipes underwent in fact event changes in the Mediterranean and in the Near East, with new shapes and decorations (reflected in the typology of the

beads) and materials (possibly mirrored by the chemical composition of the glass) appearing at the start of the IA.

In Italy, Final Bronze Age (FBA) was a remarkable period of glass-working and several archaeometric papers deal with glasses of this period: the chemical composition of beads from workshops in Frattesina, together with that of other places such as the nearby Mariconda di Melara or Fondo Paviani (Veneto, Italy) has been determined, and associated with a well-defined mixed alkali glass composition called Low Magnesium High Potassium (LMHK) glass [1–6]. The chemical data suggested that this type of glass could have been produced locally, and isotopic analyses provided further clues that would place the origin of this glass in a volcanic region—possibly near Rome [7]. Several beads included in the present study have been recognized on typological bases as FBA glass. Since the production of LMHK glass took place during a period of about 200 years, surely in different workshops, some compositional variability is expected [8]. In addition, evidence of Bronze Age Low Magnesium Glass (LMG) in Sardinia [9] and in a workshop waste at Fondo Paviani [10] also emerged.

The composition of a sample dated to the thirteenth–twelfth century BC from northern Germany [11, 12] and of other samples found in many places in Europe, Asia, and Africa [2, 5, 13–17], showed that HMG was used throughout the Bronze Age and beyond. In the Middle East, during the IA, HMG was gradually replaced by LMG produced with sodium-rich evaporites instead of plant ash [16, 18, 19], leading to an evident change in glass-making technology.

As glass from IA contexts in *Etruria* and *Latium* has not been extensively considered yet from an archaeometric point of view, this paper aims at contributing new compositional data to support the archaeological interpretation of the complex historical reality of the area. Besides investigating the compositional features of apparent LBA glass found in EIA contexts, the present study also investigates the above-mentioned technological transition as mirrored by the chemical composition of several typological varieties of glass beads. Typology is the first evidence that is considered by the archaeologists when discussing glass beads, therefore the typological frame has been kept throughout this work. The beads were selected in order to mirror the variety of the blue-green glass finds from IA contexts in Central Italy. Several bead types included in this work were probably made on the Italian peninsula (see Sect. "Archaeological glass beads"), therefore, the determination of their composition would reveal whether the raw glass was imported, thus deepening significantly our knowledge of the glass supply in central Italy at that time.



Fig. 1 Positions of the archaeological sites where the glass samples were found. The map outlines the present-day administrative regions in Italy. The sites are the following: 1 – Vulci; 2 – Cerveteri; 3 – Veio; 4 – Capena; 5 – Terni; 6 – Osteria dell’Osa; 7 – Marino; 8 – Sermoneta; 9 – Verucchio

Most of the beads involved in this study were not allowed to leave the museum premises, therefore a two-stage approach was employed to investigate the set of glass samples: a non-invasive, on-site campaign with portable equipment, namely digital Optical Microscope (OM), Fibre Optics Reflectance Spectrometer (FORS), and two portable X-Ray Fluorescence (p-XRF) spectrometers. Then, a subset of eighteen samples was analysed in the laboratory with Scanning Electron Microscopy coupled with Energy Dispersive Spectrometry (SEM-EDS), micro-Raman spectrometry (μ -Raman), and Laser Ablation Inductively Coupled Plasma Mass Spectrometry (LA-ICP-MS). The sequence of the scientific techniques allowed a broad compositional screening of the beads included in this research, while still achieving the depth of insight that was possible only in the laboratory. The analytical capability of the outlined procedure yielded data that were informative for silica and flux sources employed in the glass-making and allowed the investigation of the colouring and opacifying agents. The accuracy of the quantitative information was carefully tested in this work, since it is a prerequisite that enables the discussion of the data in the frame of the elemental compositions already available in the literature for LBA and IA glass.

Materials and methods

Archaeological glass beads

The selected set of glass beads (Fig. 2) includes samples from eight typological groups and from nine archaeological contexts (Table 1). The reader shall refer to these two elements (i.e.: Fig. 2 and Table 1) whenever specific beads are mentioned throughout the text. In addition, the main features of the eight typological groups are outlined in Additional file 1: Table SI1. Each group poses specific questions, which can be addressed by complementing with the chemical characterisation presented in this work the information already known from the archaeological examination of the beads (i.e.: the typological classification) and the archaeological context.

A description of the beads selected in this work according to their typological classification and the specific archaeological questions associated with each group are given below, whereas the general frame and the goals of the overall research have been presented in the introduction.

Group 1. Beads of Final Bronze age typology

Besides being found in EIA funerary contexts, these beads can be attributed to an earlier production based on typological features. The group includes, in particular, two forms that are specific to the Final Bronze Age (FBA): the horned stratified eye bead (*perla a occhi stratificati*



Fig. 2 Glass beads (or bead fragments) included in this study. The samples are divided into the typological groups described in the text. Photographs presented with permission of Museo Nazionale Etrusco di Villa Giulia and Museo delle Civiltà

cornuti, *Pfahlbaunoppenperle*) and the barrel-shaped bead decorated with a white spiral around the body (*perla a botticella con decorazione spiraliforme*, *Pfahlbautönnchen*). Both types have been frequently found in Italy and in other archaeological sites north of the Alps, and particularly in Swiss pile-dwelling settlements [20–22]. They are among the bead typologies manufactured in Frattesina di Fratta Polesine (Veneto, Italy) during the FBA. In particular, the barrel-shaped beads were found in Frattesina with much greater colour variations beyond

Table 1 List of the samples and their archaeological contexts. The typological groups (first column) are described in the text

Sample			Context					
Group	Inventory number	Name	Grave	Site	Locality	Absolute date	Relative date	Refs
1	59944c-59944o	VG25	Bronzetti Sardi	Vulci	Cavalupo	850–825 BCE	Early Iron Age IB	[27]
1	59944c-59944o	VG26	Bronzetti Sardi	Vulci	Cavalupo	850–825 BCE	Early Iron Age IB	[27]
1	59944c-59944o	VG29	Bronzetti Sardi	Vulci	Cavalupo	850–825 BCE	Early Iron Age IB	[27]
1	69849.014	PG84	Tomb 57 bis	Sermoneta	Caracupa	770–720 BCE	Early Iron Age II	[44]
1	73118.001	PG87	Tomb 90	Sermoneta	Caracupa	770–720 BCE	Early Iron Age II	[45]
1	109399.029	PG112	Tomb 10	Roma	Osteria dell'Osa	800–750 BCE	Early Iron Age II	[46]
1	109310	PG167	Tomb 82	Roma	Osteria dell'Osa	750–720 BCE	Early Iron Age II	[46]
1	109312.002	PG169	Tomb 82	Roma	Osteria dell'Osa	750–720 BCE	Early Iron Age II	[46]
2	59944c-59944o	VG22	Bronzetti Sardi	Vulci	Cavalupo	850–825 BCE	Early Iron Age IB	[27]
2	59944c-59944o	VG23	Bronzetti Sardi	Vulci	Cavalupo	850–825 BCE	Early Iron Age IB	[27]
2	59944c-59944o	VG24	Bronzetti Sardi	Vulci	Cavalupo	850–825 BCE	Early Iron Age IB	[27]
2	91419.001	PG158	Tomb 91	Terni	S. Agnese, Acciaierie	950–800 BCE	Early Iron Age I	[47]
2	91419.001	PG159	Tomb 91	Terni	S. Agnese, Acciaierie	950–800 BCE	Early Iron Age I	[47]
2	91419	PG161	Tomb 91	Terni	S. Agnese, Acciaierie	950–800 BCE	Early Iron Age I	[47]
3	69688	PG65	Tomb 8	Sermoneta	Caracupa	770–720 BCE	Early Iron Age II	[44]
3	109407.002	PG121	Tomb 10	Roma	Osteria dell'Osa	800–750 BCE	Early Iron Age II	[46]
3	109409.002	PG122	Tomb 10	Roma	Osteria dell'Osa	800–750 BCE	Early Iron Age II	[46]
3	67722	PG160	No context	Terni	S. Agnese, Acciaierie	950–700 BCE	Early Iron Age I/II	[47]
3	73131	PG166	Tomb 91	Sermoneta	Caracupa	770–720 BCE	Early Iron Age II	[45]
4	16530	VG106	Tomb 104	Capena	Saliere	800–700 BCE	Early Iron Age II	[48]
4	109399.011	PG109	Tomb 10	Roma	Osteria dell'Osa	800–750 BCE	Early Iron Age II	[46]
4	109399.015	PG110_1	Tomb 10	Roma	Osteria dell'Osa	800–750 BCE	Early Iron Age II	[46]
4	109399.025	PG111	Tomb 10	Roma	Osteria dell'Osa	800–750 BCE	Early Iron Age II	[46]
4	165946	PG138	Tomb 29	Cerveteri	Furbara, Caolino	750–720 BCE	Early Iron Age II	[49]
5	31614	PG162	No context	Verucchio	Fondo Ripa	775–725 BCE	Early Iron Age II	[50]
5	31614.001	PG163	No context	Verucchio	Fondo Ripa	775–725 BCE	Early Iron Age II	[50]
5	31614.002	PG164	No context	Verucchio	Fondo Ripa	775–725 BCE	Early Iron Age II	[50]
6	68243	PG39	Tomb 14	Veio	Vaccareccia	700–650 BCE	Early Orientalising	[51]
6	74316	PG88	Tomb 61	Capena	S. Martino	675–625 BCE	Middle Orientalising	[52]
6	74344	PG89	Tomb 60	Capena	S. Martino	675–625 BCE	Middle Orientalising	[52]
6	87603	PG97	Tomb 21	Marino	Riserva del Truglio	730–600 BCE	Orientalising	[53]
7	68408	PG59	Tomb 24	Veio	Vaccareccia	700–650 BCE	Early Orientalising	[51]
7	68409	PG60	Tomb 24	Veio	Vaccareccia	700–650 BCE	Early Orientalising	[51]
8	68231.001	PG33	Tomb 13	Veio	Vaccareccia	750–730 BCE	Early Iron Age II	[51]
8	68416	PG63	Tomb 24	Veio	Vaccareccia	700–650 BCE	Early Orientalising	[51]
8	109400	PG116	Tomb 10	Roma	Osteria dell'Osa	800–750 BCE	Early Iron Age II	[46]
8	165929	PG136	Tomb 26	Cerveteri	Sasso di Furbara, Caolino	770–730 BCE	Early Iron Age II	[49]
8	109312	PG168	Tomb 82	Roma	Osteria dell'Osa	750–720 BCE	Early Iron Age II	[46]
8	109312	PG170	Tomb 82	Roma	Osteria dell'Osa	750–720 BCE	Early Iron Age II	[46]
8	109312	PG171	Tomb 82	Roma	Osteria dell'Osa	750–720 BCE	Early Iron Age II	[46]

the simple combination of a blue matrix glass with a white decoration mostly found elsewhere (compare 76 f. in [6], with Fig. 1 in [11]).

The horned eye beads were made by applying four portions of white glass onto a coiled coloured bead body, and topping them with another layer of coloured glass,

thus creating a typical “eye” protruding from the bead body (pl. 121–122 in [23]; 78 nos. 21–22 and 93–95 in [6]). With some variations, the beads with four layered eyes were the most common in the FBA and the easiest to identify, such as VG25 and PG84. In some instances, one or even all eyes detached from the bead body leaving

a flat (or concave) surface, on which traces of the lost decoration may be found, such as in PG87 and PG167. Both forms had a long-lasting tradition beyond the FBA (ff. 85–91 in [6]; Fig. 2 in [24]), and might have been produced in Italy as early as in the thirteenth century BCE (*Bronzo Recente*) from a High Magnesium rust-Brown Glass – HMBG [25] (f.177 pl. LVIA in [21]; in summary ff.81, 85 in [26]).

The beads included in Group 1 were found in the inhumation graves of two Latial necropolises (namely Osteria dell'Osa and Sermoneta-Caracupa) and in one famous cremation burial in the Etruscan necropolis of Vulci-Cavalupo named “Tomba dei Bronzetti Sardi” because it contained three imported Sardinian bronzes [27]. The samples considered here (namely VG25, VG26 and VG29) were found in this tomb with other beads, most of which showed signs of secondary burning reflected in changes of both colour and texture. Two beads from Osteria dell'Osa have been included in this group: one is a conical, irregularly wound green bead from tomb 82 (PG169) and the other is a fragment of a green bead with a white spot decoration (PG112). The latter corresponds to type 18 from Frattesina [6], for which an FBA-typical composition can be assumed. Both beads have a slightly translucent turquoise-green matrix glass, which is unusual for the EIA. The main goal of the analysis of these samples would be to check their correspondence to an LBA glass compositions.

Group 2. Small ring beads

(*Perlina ad anello; feine Ringperle*). This set includes dark, blue, and reddish ring-shaped (in some instances also oblate) beads. Small ring beads, made in series by winding hot glass around a mandrel, played a prominent role within the burial customs of both FBA and EIA [28] in Italy, as more than 95% of the beads from Frattesina were undecorated ring beads (pl. LVII in [21]; 71f. Figure 1 and Fig. 12 in [6]). Moreover, translucent turquoise ring beads were found in large numbers beyond the Frattesina area and throughout the Italian peninsula ([29], p. 19 with fig. [30]; f. 81 in [6]), also in some IA graves (pl. 11, 74–76 in [31]). The compositional characterization of the beads included in this group would contribute some elemental data to the multidisciplinary framework aimed at tracing the circulation of these beads during FBA and IA.

Group 3. Green beads with black-yellow decoration

This group includes five beads from the necropolises of Osteria dell'Osa, Sermoneta-Caracupa, and S. Agnese-Acciaierie (Table 1). Three are ring-shaped beads with two or three spiral eyes (*perla verde con occhi a spirale nero-gialli; grüne Perlen mit gelb-schwarzen Spiralau-gen*). These decorations were unique for the EIA and were

obtained by assembling through heat two glass portions of different colours, which were afterwards drawn into a twisted *reticella* thread (p. 30 Fig. 12 [32]). Two or three portions of this thread were then placed on the bead body, protruding plastically (such as in PG122) or sinking smoothly in the bead body (PG166). The second type is a smaller ring-shaped or cylindrical bead, on which a black (and maybe yellow) thread was fused as a line without encompassing the entire circumference of the bead body (*piccola perla verde con filo nero(-giallo?); kleine grüne Perle mit schwarzer(-gelber?) Fadendekoration*). The fragmented bead considered here only shows the shallow groove of the now missing decoration (PG121), whereas the other bead (PG65) keeps some remnants of the decoration thread. The overall appearance of the beads sets them apart from other known EIA bead types. Their chemical characterisation can contribute further knowledge regarding their origin.

Group 4. Cu-Co coloured eye beads

Eye beads (*perla blu con occhi bianchi ad anello semplice; blau-weiße Ringaugenperle*) were among the earliest, longest-lasting and most widespread beads from the EIA [33]. The decoration normally consisted of three “eyes” shaped as rings of white glass sunken in the hot blue glass matrix, and it was sometimes lost in eye beads (but not for the beads considered in this study). Besides the typological attribution to eye beads, this small group of beads was highlighted during previous analyses performed on a larger set of eye blue beads coloured by cobalt [34], as both copper and cobalt played a role in the blue colour of these samples. Differences in size, colour, opacity, and technique of production already suggested that different compositions would be detected within this group [34]. Nevertheless, this specific set of blue beads attracted attention because they are one of the first examples of LMG in Central Italy, and they are considered here for a further compositional insight.

Group 5. Tubular beads

(*Vago o pendente a tubetto; Röhrenperle*). These rare and extraordinary beads from Verucchio were wound on a metal rod, similarly to simple ring beads. Then, they were decorated with a hot white glass thread spiralled more than 20 times around the body and “combed” four to five times with a metal tip or a knife to create an arched or herringbone pattern [35]. The decorative thread was lost in the samples considered here, changing their original appearance. Similar beads were found only in two other graves of the Lippi necropolis in Verucchio, dated back to the middle of the eighth century BCE (19–20 type 13A, pl. 31, pp. 228–230 in [31]). The determination of their

composition would add some information for their interpretation, as their rarity led to a general lack of the archaeological inference.

Group 6. Melon beads

(*Perla costolata o a melone; Melonenperle*). Three spherical melon beads are included in this group. The technique for producing these beads was already known in the LBA and the earliest IA (type 9 in [6]; pp. 37–39 in [36]; Fig. 1 in [37]). They became more common in the sixth–fifth century BC, and two workshops for their production were documented by archaeological evidence [38, 39]. The spherical beads were formed on a rod and their hot body was then treated with a tool, such as the back of a knife, to produce the relief form. The elongated pendant PG97 was obtained with a similar technique, but the thin bronze rod inside suggests that it was used for suspension. Also for this group, the question of their origin arose; therefore, the chemical characterization would allow us to set these samples in the broader frame of information for blue glasses.

Group 7. Fibula bow beads

(*Vago per il rivestimento dell'arco di fibula; Fibelbügelperle*). The *sanguisuga* (leech-shaped) blue beads PG59 and PG60 were specially made for the decoration of brooches. The body has impressions of a round model on the underside, which pushed the "belly" into width, but the beads must have already been wound on a curved rod (pp. 58–61 photos on CD in [40]; Fig. 7 in [41]). They were decorated with a yellow glass that was wound around the body and "combed" into a herringbone pattern while the matrix glass was still quite hot, as the decoration glass sunk completely into the matrix. This forming procedure distinguishes the fibulae beads of this group from those, much more common and larger, found in the region of Bologna and Verucchio [40, 41]. The shaping technique that characterises the beads considered here was found only in a few other cases in Veio (from the same tomb, but with brown glass), as well as in Narce, Falerii, Capena, and a unique green and red example in Picenum (cat. no. 154–161 in [40]; Fig. 8 in [41]). Archaeological and technical evidence suggested that they could have been made somewhere in Southern Etruria, perhaps *Ager Faliscus*; therefore, their elemental composition could clarify if they were made with imported or local glass. The comparison with the composition of the probably imported bead (PG63, Group 8), found in the same grave, would also be of particular interest for the interpretation of these bow beads.

Group 8. Blue spherical or ring-shaped beads

This group includes an assorted set of blue beads. Three thick ring-shaped beads were from Osteria dell'Osa. Two of them (namely PG168 and PG171) were deep turquoise and translucent, and a few similar beads were found in archaeological sites widely scattered throughout Italy [33]. The third bead from the same tomb (PG170) was made of turquoise-light blue opaque glass. Opaque, turquoise glass coloured with copper was used in Egypt in the Bronze Age [42], but it was very unusual for EIA contexts in Italy. Incidentally, an opaque turquoise decoration glass on a bird bead found in the same tomb (not included in this present sample set) is also very unusual [43]. The rest of the beads of this group (PG33, 63 and 116) are made of translucent blue glass. Finally, PG136 is a small fragment that was (tentatively) assigned to this group based on colour/translucency proximity.

The determination of the chemical compositions of these beads would support their contextualisation in the general frame of glass beads production and exchange.

Techniques and equipment

The list of the samples, with the analytical techniques that were employed for each of them is available in Additional file 1: Table SI2.

Optical microscopy (OM)

A Dino-Lite AM4815ZT–Edge digital microscope was used to examine the beads to properly document their characteristics and select the analytical spots. Digital images at 20X and 100X were acquired to enhance the overall quality of the photographic documentation available for the investigated beads.

Fibre optics reflectance spectroscopy (FORS)

This technique was employed to non-invasively detect the colouring agents. It was not possible to find suitable conditions to record informative spectra for all the samples, and those with pronounced surface weathering did not show any characteristic spectral feature. The light of an Ocean Insight HL-2000-HP-FHSA 20 W Tungsten halogen source was transmitted through a 2 m long reflection/backscatter fibre optics bundle ending with a probe of 400 μm core diameter and 6.35 mm ferrule diameter. Samples were fixed on a sample holder, adjusting the angle of the probe to (circa) 45°, in order to capture the diffused light and exclude the reflected component. With this arrangement, the analytical spot was a few mm^2 , which was often suitable to test the main colour of the bead, but not the smallest decorations. Diffuse light was transmitted to an Ocean Insight QEPro CCD detector with HC1 grating, operating from 248 to 1038 nm with an optical resolution of 6.78 nm FWHM.

The system was calibrated using a high reflectivity Spectralon reference. Integration time was set from 0.019 to 0.029 s and 40 scans (or more) were averaged for single spectrum acquisition. Several spectra were acquired in different parts of each bead. Diffuse reflectance spectra were then normalised to 100%, in order to enable a direct comparison between the absorption features of glasses with different colour saturation.

Portable X-Ray fluorescence spectroscopy (p-XRF)

Two p-XRF spectrometers were used. The ELIO unit (XGLab S.R.L. Milan, Italy) was employed to analyse the “PG” series of the samples. It was equipped with a Rh anode source with the beam focused about 1.2 mm diameter, and a 25 mm² Silicon Drift Detector (SDD). The settings were as follows: acquisition time: 90 s; current: 40 μA; voltage: 40 kV.

The “VG” set was analysed by an in-house-built portable XRF spectrometer developed by the Italian National Institute of Nuclear Physics (INFN Frascati, Italy). This device is equipped with a W anode source and the beam is focused through polycapillary optics down to a spot of 300 μm in diameter. The SDD detector has an active area of 20 mm² and a resolution at Mn Kα of 173 eV. The instrument parameters were set as follows: time: 200 s; current: 80 μA; voltage: 40 kV.

All the p-XRF spectra were fitted to obtain elemental concentrations using PyMCA software [54]. The optimization of the analytical procedure for archaeological glass and the tests performed to check the quality of the data for the equipment was discussed throughout in a previous publication [55]. p-XRF results were treated with Instant Clue open-source data analysis software [56] applying Principal Component Analysis (PCA), which was used to check the heterogeneity within the dataset for averaged compositions of the samples (excluding the decorative parts). Values below the estimated Limit of Quantification (LOQ) were set to 0 and both row and column Z-score standardisation was used for data pre-treatment.

(Variable pressure) Scanning Electron Microscopy coupled to Energy Dispersive Spectrometry ((VP)-SEM-EDS)

Eight samples were analysed with this technique – five were prepared as polished cross sections and analysed under high vacuum, and three (PG39, VG22 and VG106) were placed without any preparation in the sample chamber and analysed at low-vacuum conditions (50 Pa). The equipment was a JEOL (Akishima, Japan) JSM-IT300LV coupled to an Energy Dispersive Spectrometer with an SDD detector (Oxford Instruments, Abingdon, UK). Spectra were recorded using the following conditions: 1) voltage: 15 kV; 2) current: approx. 2 mA; 3) acquisition

time: 40 s; 4) working distance: 10 mm. The compositional data on cross sectioned samples were collected from square areas of approximately 10 μm side at 5000×. Data from five areas were averaged to calculate the mean bulk composition (normalised to 100%) and the standard deviation. Besides gaining information on the composition of the glass matrix, these data were employed to further check the accuracy of Ca concentrations determined by p-XRF, as these were used as the internal standard in the LA-ICP-MS analyses. Inclusions (if any present) were analysed by focussing the electron beam on the target particle, collecting qualitative elemental information from the investigated spots.

Micro Raman spectroscopy (μ-Raman)

Raman analyses were carried out employing a LabRAMHR Evolution (Horiba, Kyoto, Japan) spectrometer, equipped with a Peltier-cooled charge-coupled device detector (CCD), a He–Ne (633 nm) and an Ar (488–514 nm) laser, a BH2 microscope (Olympus Corporation, Tokyo, Japan) and an Ultra-low wavenumber module, which allows Raman spectroscopic information in the sub-100 cm⁻¹ region with a spatial resolution of 1 μm and a spectral resolution of about 1 cm⁻¹. Four objectives, namely 20X, 50X and 100X (Leica DMLM microscope) and a long working distance 50X one (Olympus (Japan)), were used to focus the laser beam on the samples. The instrument was calibrated on the 520.5 cm⁻¹ peak of a Si (111) standard. The analytical parameters were adjusted in order to optimize the signal-to-noise ratio, constraining the laser power below 25% (514 nm excitation) and 75% (633 nm excitation) to avoid damaging the sample. Spectra were acquired employing an 1800 gr/mm grating in the spectral range of 60–1560 cm⁻¹. A linear baseline was subtracted from the raw spectra using the software LabSpec6 (Horiba, Kyoto, Japan) setting anchors at ca. 60, 300, 700, 800, and 1300 cm⁻¹. Deconvolution of the bands was then performed using the curve fitting application Fityk [57].

Laser Ablation – Inductively Coupled Plasma – Mass Spectrometry (LA-ICP-MS)

Seventeen samples (Additional file 1: Table SI2) were analysed by a NexION 300×Perkin-Elmer (Waltham, USA) ICP single quadrupole mass spectrometer coupled to an ESI NWR 213 laser ablation system (ESI New Wave Research Co., Cambridge, UK). The concentrations of 38 elements were determined. The measured masses are given in Table 2, which also shows the accuracy and precision of the quantitative results tested on certified reference materials. In addition, Table 3 reports the settings applied during the acquisitions. The preliminary laser shots allowed the micro-sampling of the pristine glass

Table 2 Average recoveries and relative standard deviations ($n=69$) of QC standards during LA-ICP-MS sessions: CMOG A for major and minor elements, NIST614 for trace elements

CMOG A			NIST614		
	Average recovery (%)	RSD (%)		Average recovery (%)	RSD (%)
^{23}Na	97	2.2	^{85}Rb	99	5.2
^{24}Mg	100	5.9	^{88}Sr	98	0.3
^{27}Al	88	3.1	^{90}Zr	97	3.4
^{28}Si	92	3.2	^{133}Cs	97	1.6
^{39}K	80	23	^{138}Ba	102	3.4
^{48}Ti	102	8.6	^{139}La	87	8.2
^{51}V	99	1.3	^{140}Ce	99	6.1
^{55}Mn	115	7.6	^{144}Nd	97	9.2
^{57}Fe	91	6.4	^{147}Sm	107	5.2
^{59}Co	96	0.7	^{153}Eu	78	0.1
^{60}Ni	111	1.2	^{158}Gd	107	4.8
^{63}Cu	74	37	^{159}Tb	100	3.4
^{64}Zn	103	9.6	^{163}Dy	98	3.2
^{75}As	86	2.4	^{166}Er	112	12
^{118}Sn	87	8.3	^{174}Yb	109	6.4
^{121}Sb	96	11	^{175}Lu	105	4.7
^{208}Pb	85	4.8	^{177}Hf	101	0.6
			^{205}Tl	98	1.0
			^{232}Th	95	6.3
			^{238}U	100	0.7

under the surface and the experimental settings ensured the highest sensitivity of the equipment, thus depressing the formation of interatomic interferences and double-charged ions. For each colour on one single glass bead, 3 to 5 acquisitions were obtained. Quantification was then performed using ^{44}Ca as the internal standard, relying on the concentration values obtained for this element through p-XRF. The data from each sample were

averaged and normalised to 100% based on major and minor elements (expressed as oxide wt. %).

At the beginning and at the end of each analytical session, as well as after every 5 samples, blank values (acquisition of the gas flow without ablation) and shots on the reference materials were carried out to check the accuracy and highlight possible drift. The primary standard used for calibration was NIST612, and the QC standards were CMOG A (major and minor elements) and NIST614 (trace elements). The values of Mg, K and Ti were found to be systematically over- or underestimated. It was decided to offset the biases of analyses through the mean value obtained for these elements for certified values of CMOG B, C and D reference materials.

Results

Fibre Optics Reflectance Spectroscopy (FORS)

The detailed results from the FORS investigation are reported as Additional file 1: Table SI3, whereas exemplary patterns are reported in Fig. 3. The interpretation of the spectra was supported by the work of Micheletti et al. [58] and the references therein.

A large number of the beads within our sample set yielded spectra with peak reflectance in the blue-green region, with the typical absorption band of Cu^{2+} ions in octahedral coordination (Fig. 3, top). All the beads from Groups 3, 5 and 7, and most of the beads from Groups 6 and 8, featured the band of Cu^{2+} , although the feature is variously scattered throughout all the typological groups. Some beads also feature other bands in addition to that of Cu^{2+} : a weak band of Fe^{3+} at 380 nm for PG136 and the Fe^{3+} band at 450 nm for PG63; moreover, spectral features would indicate a possible presence of Mn^{3+} in the samples of Group 7, to be confirmed through other elemental techniques.

Another group of spectra (Fig. 3, middle) mostly consisted of representatives of Groups 2 and 4, but also

Table 3 LA-ICP-MS settings

Laser settings		Plasma settings	
Type	213 nm Nd:YAG		
Energy at the sample (For 100 μm spot and 20 Hz)	3.2 mJ	Nebuliser gas	Ar, 0.7 L/min
Mode	Continuous pulse	Auxiliary gas	Ar, 1.2 L/min
Energy	80%	Plasma gas	Ar, 15 L/min
Repetition rate	20 Hz	RF power	1550 W
Spot size	80 μm	Acquisition mode	Peak hopping
Ablation time	60 s	Dwell time for the detector	20 ms (5 ms for ^{23}Na , ^{27}Al , ^{28}Si and ^{44}Ca)
Gas flow	He, 1L/min	Detector readings per acquisition	40

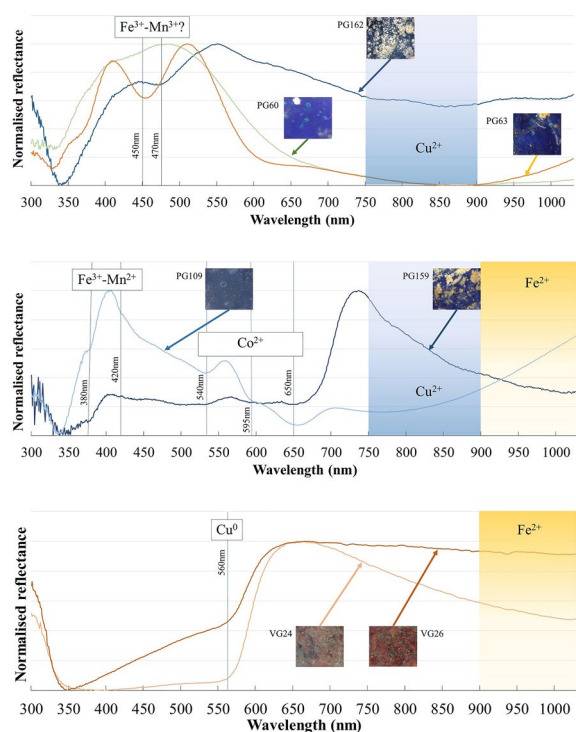


Fig. 3 Representative FORS spectra with bands for spectral interpretation and images for colour/texture reference

included spectra of other typological groups, namely: VG23 and 106, PG109, 111, 158, 159, and 171. These spectra featured Fe^{3+} bands at 380 nm and 420 nm, which possibly also indicated the presence of Mn^{2+} , and the characteristic Co^{2+} triplet, detected at 540, 595, and 650 nm.

Within this general picture, different trends were highlighted in the NIR region: samples of Group 4 mainly featured a pronounced Cu^{2+} band, while other samples mostly showed the Fe^{2+} one. In addition, a division in the reflectance at around 400 nm emerged: PG158, 159, and VG106 showed low reflection in that region, having their maxima after 700 nm; samples PG138 and VG23 showed average levels of reflectance and the rest of the samples reflected strongly at about 400 nm (Fig. 3, middle). Such differences could be caused by the different relative contents of Fe^{3+} and Mn^{2+} in the glass matrix [59].

Reddish glasses (VG24, 25, 26, 29) showed the Cu^0 band at approximately 560 nm, with some samples featuring the broad Fe^{2+} band in the NIR region (Fig. 3, bottom), supporting the evidence of heating under reducing conditions.

No information was obtained by this technique for the small decorative parts of white or yellow glass, as the spectra did not feature any characteristic band except those from the bulk of the bead.

Portable X-Ray Fluorescence (p-XRF) spectrometry

On-site p-XRF analyses were crucial for tracing the compositional links among different samples, which were then used to determine if the sample subsets that were allowed to be analysed in the laboratory could properly represent the whole set of samples.

The composition of the samples determined in this work by p-XRF is reported as Additional file 1: Table SI4. For sake of comparison, the data already published for the Co–Cu coloured beads of Group 4 [34] are also included. The results of a preliminary inspection of the p-XRF data with PCA (the first three PCs accounted for 59.94% of explained variance) are reported in Fig. 4.

The typological groups were separated by PC1, with K_2O and CaO playing the main role. Samples of groups 1 and 2 featured higher levels of K_2O than the samples included in the other groups, with Group 1 reaching the highest levels (4–5 wt% of K_2O), and Groups 3 and 7 with the lowest (some 1.5–3% of K_2O). For all the other samples, the K signals were mostly below the LOQ (i.e. 1.2% K_2O), with some exceptions in Group 8 (PG33, 63 and 170). The CaO values showed a different picture: Groups 2 (Terni samples only), 3, 4, 5, and 8 featured the highest concentration, whereas Groups 1 and Vulci samples of Group 2 featured the lowest ones within the whole sample set.

For PC2, the key elements were Ti, Zr, Cu, Mn, and Sn, although no specific separation emerged for this PC. PC3 accounted for a separation due to the different contents of Co and Ni.

The PCA plots in Fig. 4 highlighted that composition mostly reflected typology, with few noticeable exceptions. PG112 (Group 1) joined Groups 5, 6, and 8, confirming the results in [34]. Similarly, PG169 (Group 1) was more associated with Group 3. Group 8, though being placed along a trend of PC2, proved to be quite heterogeneous from a compositional point of view. Groups 1 and 2, although broadly dispersed in the plots, were the only ones with positive values for PC1. Tubular beads, although typologically well distinguishable, were closely associated with Groups 6 and 8 on compositional basis.

Besides giving a general overview of the distribution of the typological groups from a compositional perspective, the purposes of the p-XRF analyses was to track the representativeness of the smaller set of samples analysed in the laboratory, as all the groups, except Groups 5 and 7, had some representatives in the subset investigated by micro-invasive techniques. Samples in the bottom right quadrants of the PCA plots in Fig. 4, e.g. the reddish glasses from the Bronzetti Sardi tomb, were underrepresented and it was not possible to obtain these samples to be analysed in the laboratory. This issue shall be kept

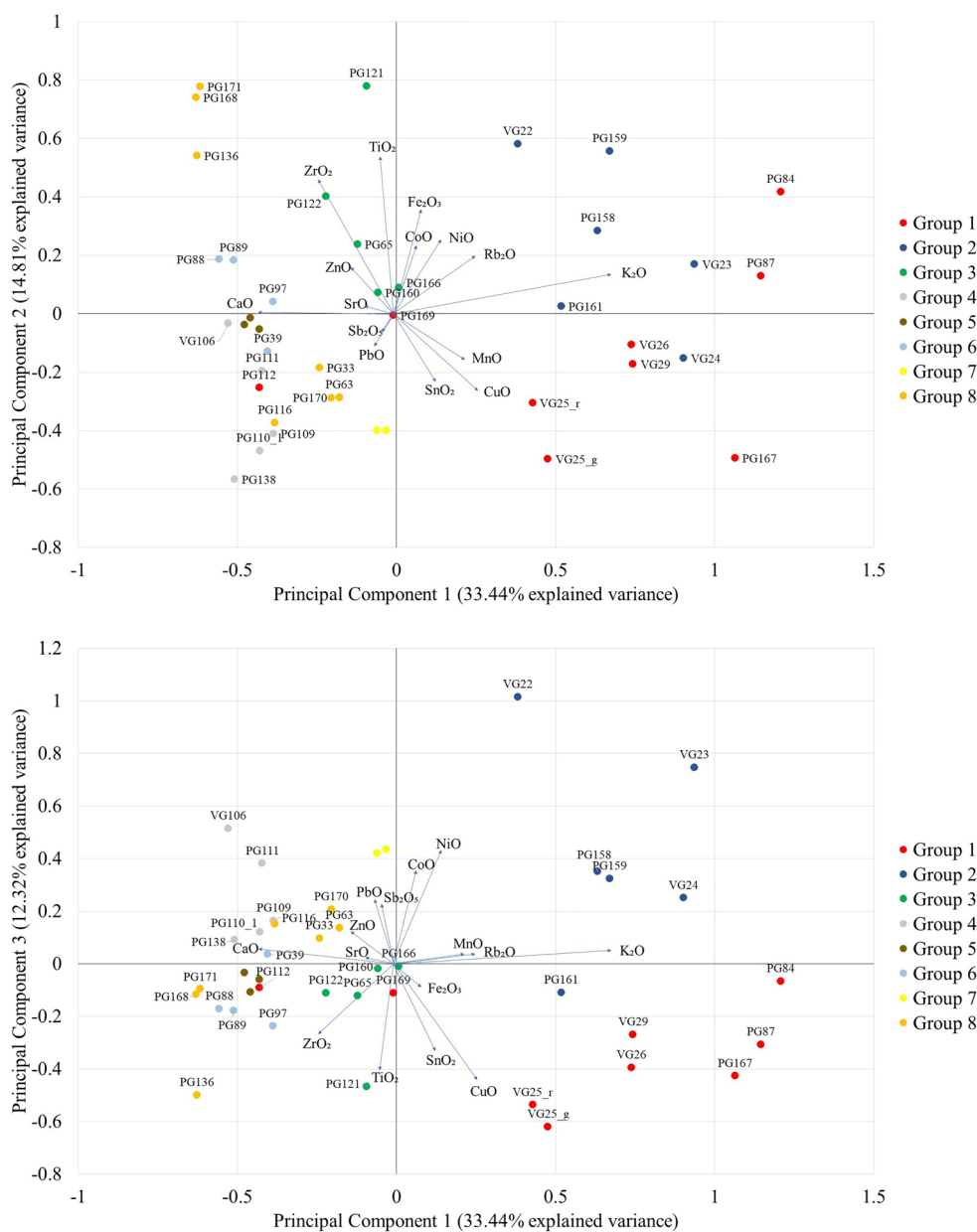


Fig. 4 Biplot of PCA for p-XRF data. PC1 vs PC2 (top) and PC1 vs PC3 (bottom). Data on decorative parts are not included in the plots

into consideration in the discussion of the data reported in Sect. “Discussion”.

A deeper insight into the general trends shown by PCA on p-XRF data was obtained from some binary plots relevant to glass characterisation (Fig. 5). Fe₂O₃ vs TiO₂ plot showed that samples PG88, 89 (Group 6) and 136 (Group 8) featured more Ti than the rest of the samples in their groups, without a proportional gain in Fe. CaO vs SrO plot suggested the same trend line for almost all the samples, and different typological groups showed somewhat

different levels of these elements. Regarding the reddish samples from Group 1, they all were within the concentration ranges of Groups 1 and 2, leading us to assume that the compositions of the samples from Groups 1 and 2 would be representative of a same type of glass. Group 5 samples were associated with Groups 4, 6 and 8. PG63 was the sample closer to those of Group 7 (fibula bow beads) on compositional bases, despite their evident typological difference. These assumptions on compositional similarity allowed us to broaden the discussion of

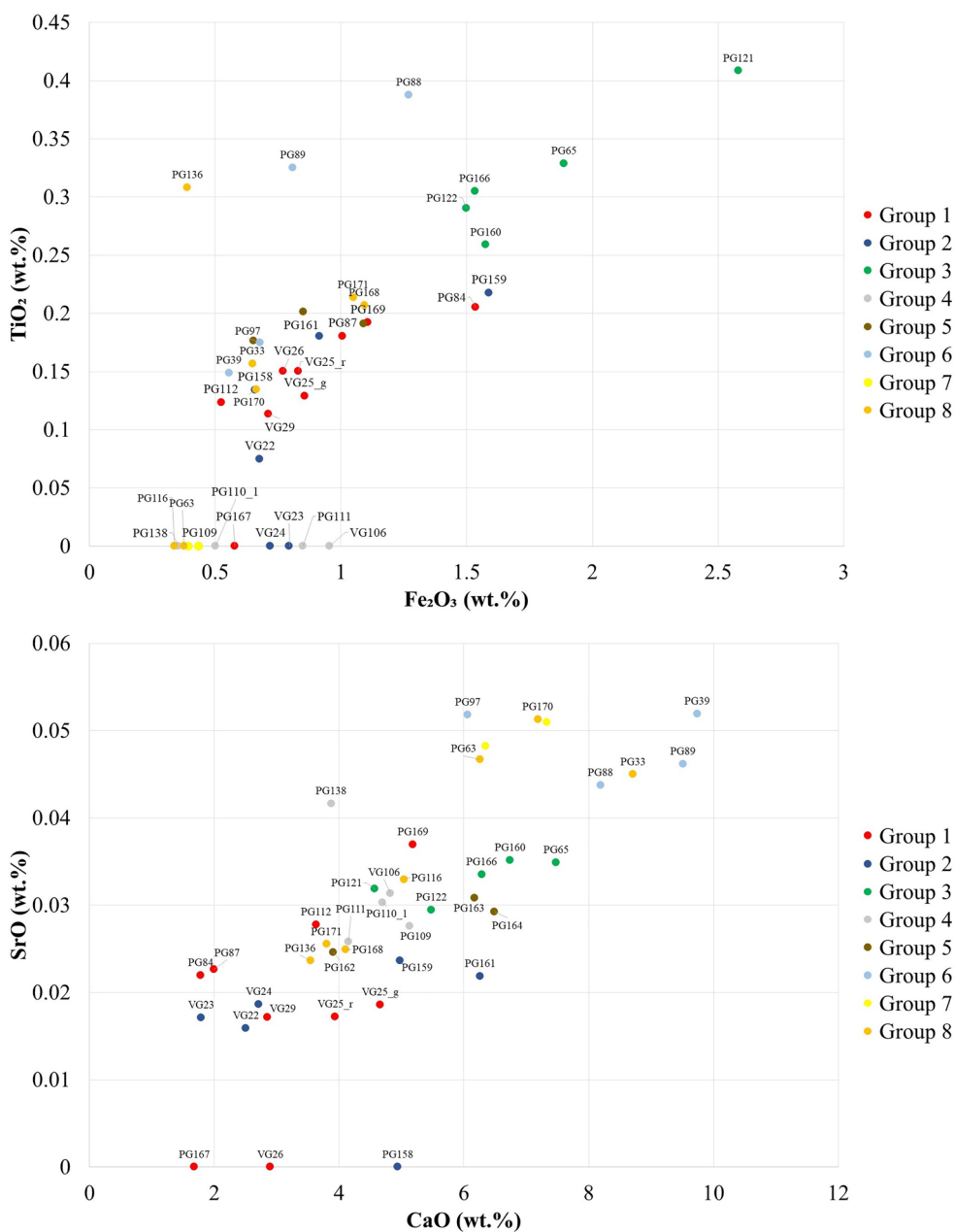


Fig. 5 Binary plots of p-XRF data. Fe_2O_3 vs TiO_2 (top) and CaO vs SrO (bottom)

the data from samples that were analysed in the laboratory to those analysed in the museum with a different analytical approach.

The small dimensions of the decorations (both in thickness and in width) did not allow the instrument to capture the sole response from these glasses, but some elemental evidence was collected from the opacifiers.

Ca and Sb peaks were high in the white decorations of Group 4, suggesting that calcium antimonates, already documented in Egypt since the LBA [60], were present in the white glass. This was not the case for Group 1 samples, where Sb was not detected in the white parts, although high levels of Ca were apparent for VG25 and 29. In the yellow-coloured parts (present on the beads from Groups 3 and 7), signals of Pb and Sb suggest the presence of lead antimonates to give both colour and

opacity. The dark decorations did not show any significant variation in the composition when compared to the main body of the same bead.

(Variable pressure) Scanning Electron Microscopy coupled to Energy Dispersive Spectrometry ((VP)-SEM-EDS)

The composition determined by SEM-EDS, either in cross sectioned samples or on the untreated surface of the bead, are visualized in Fig. 6 with the primary aim of showing the content of alkali and alkali-earth. Na₂O prevails over K₂O in all the samples prepared as cross-sections. This evidence, in addition to the low levels of MgO, indicates the use of a mineral source of flux. PG121 – the only representative of Group 3 that was analysed with this technique—featured high concentrations of alkali-earth oxides and more K₂O than the other samples, which might be suggestive of the use of plant ash as flux. Unfortunately, the data for the samples analysed in VP mode were compromised by the surface alteration of glass, but they might anyway

give an idea of the distribution of the alkali, taking into consideration that Na is more leached than K from the glass surface [61].

Inclusions were frequently present in the glass matrix, and a varied assortment of particles was observed on the surface of the beads analysed in VP mode. PG39’s surface was covered in particles rich in Sn and Pb, which size and distribution are shown in Fig. 7 (left). VG22 featured a heterogeneous surface (Fig. 7, right), having inclusions of highly variable compositions. In the white decorations of Group 4 beads, Ca and Sb-rich inclusions were detected. Cu seemed to be unevenly distributed on the surface of VG106.

SEM-EDS data were also employed to further check the accuracy of p-XRF data for calcium, since this element was employed as the internal standard for LA-ICP-MS analyses. For this purpose, 18 glass beads, including those considered in this work and featuring CaO concentration from 2 to 10% wt, were analysed as cross sections. The biplot of the data obtained by p-XRF and SEM-EDS

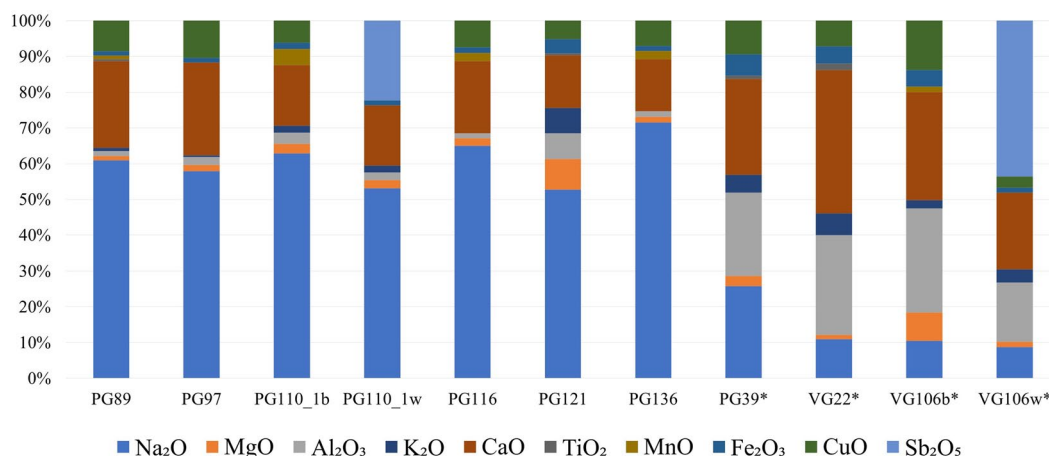


Fig. 6 (VP)-SEM-EDS data. Values of selected oxides normalised to 100% are presented. The asterisk indicate the data that were obtained in the VP mode

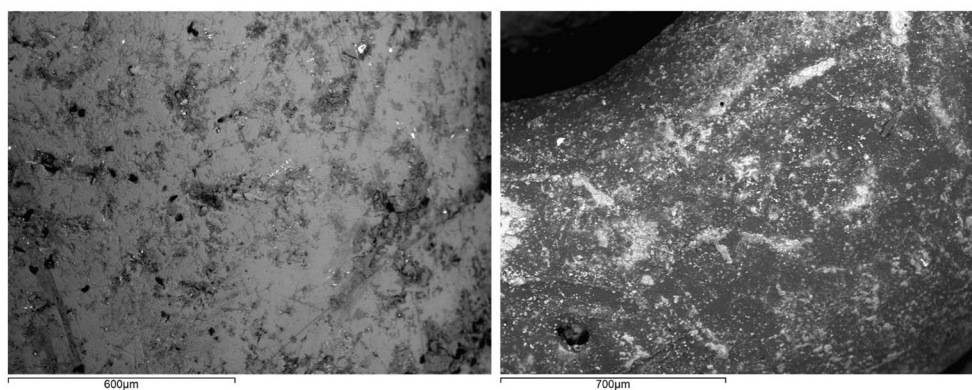


Fig. 7 BSE images of PG39 (left) and VG22 (right) surface. Heavy elements inclusions are visible as light spots

(not reported) on the same beads showed that they are randomly distributed mainly within the 20% interval around the bisector of the first quadrant, thus supporting the approach for the quantification with LA-ICP-MS.

Micro Raman spectroscopy (μ -Raman)

Raman spectra contributed two separate pieces of information: 1) the glass matrix general composition and indicative melting temperatures, obtained by the bands of Si–O bending at approximately 300–700 cm^{-1} and of Si–O stretching at 800–1200 cm^{-1} [62, 63]; 2) characterisation of the crystalline inclusions dispersed in the glass matrix [64, 65].

Not all analysed samples produced spectra with suitable Si–O signals. For those that yielded well-defined spectra, the areas of the bands were compared after Colomban (2003). The ratios of these areas were mostly within the 0.7 – 1.3 interval, which corresponds to 700–1000 $^{\circ}\text{C}$ melting temperature. The maxima of the bands of the stretching and bending Si–O modes mostly group around CMOG A and B reference glasses, i.e. soda-lime glass.

Other peaks observed in the Raman spectra highlighted the presence of $\text{Pb}_2\text{Sb}_2\text{O}_7$ in the yellow parts of PG60 and PG122 (peaks at 136 cm^{-1} and 509 cm^{-1}) and of CaSb_2O_6 in the white part of VG106 (peaks at 237, 328, 337 and the main one at 671 cm^{-1}). Calcite was detected on the surface of sample PG159 through its intense peak at 1087 cm^{-1} . Alkali sulphates were detected on samples PG122 and VG106 [64, 65]. Spectra with pronounced peaks are presented in Fig. 8.

Laser Ablation- Inductively Coupled Plasma—Mass Spectrometry (LA-ICP-MS)

LA-ICP-MS analyses yielded data on a wide set of elements in the pristine glass. In fact, an array of preliminary

laser shots removed any weathered layer, so that the unaltered glass was analysed with minimal damage to the sample. The compositional data obtained by this technique are reported in Table 4 (major and minor elements) and Table 5 (trace elements, including Rare-Earth Elements – REE).

The alkalis and MgO gave some indications to separate the samples on compositional bases (Fig. 9). Groups 1 and 2, except PG112, featured the highest concentration of K_2O (4 – 10%) and the lowest concentration of Na_2O (5 – 7%) within the dataset. On the other hand, Groups 8 and 6 (and PG112 from Group 1) showed the lowest amount of K_2O – less than 0.5% (except for the PG63) with a predominant concentration of Na_2O . The data obtained for K_2O were fully comparable with those obtained by p-XRF. Na_2O also prevailed over K_2O in Group 3, but this group, and PG63 from Group 6, featured the highest concentration of K_2O in this low-K set of samples (Fig. 9, top). Al_2O_3 vs MgO binary plot (Fig. 9, bottom) showed a less pronounced division between the groups, although a division by relative content of the two oxides emerged: high Al low Mg – Groups 1 and 2; medium Al medium Mg – Group 4, and high Mg low Al – Group 3 with PG63 (from Group 8). Group 6 and PG116 from Group 8 were characterized by having less than 1% of both Al_2O_3 and MgO.

Across all the groups, Mn was associated with Ba, which suggested the probable presence of psilomelane in the raw materials [66]. The Mn/Ba ratio was considerably higher for samples in Group 4 (where Mn is associated with Cu) and 3 samples from Groups 1, 6 and 8 – PG112, PG89 and 116 respectively, suggesting higher Ba content in the silica source (for high Mn samples $r=0.93$). The rest of the samples contained considerably less Mn, yet keeping high correlation coefficients: 0.98 for Groups 1 and 2, and 0.92 for the rest of the low Mn beads.

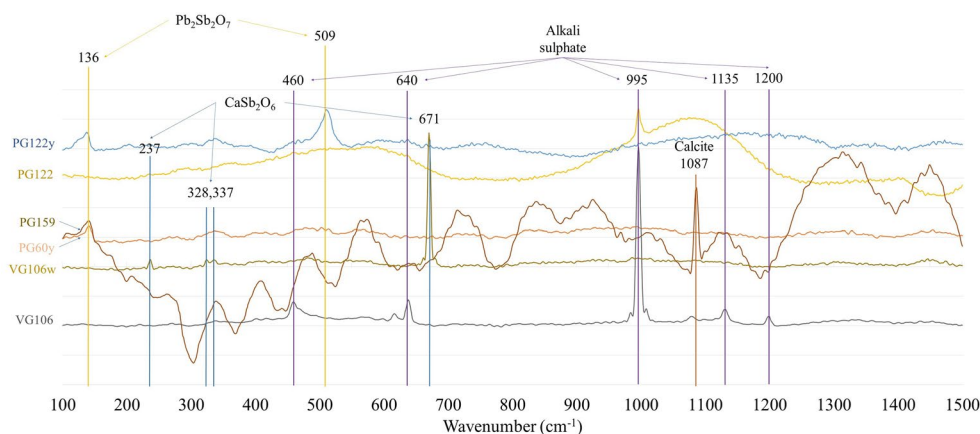


Fig. 8 Raman spectra that featured the peaks of inclusions, w – white, y – yellow. Attribution of the peaks is given by the arrows

Table 4 LA-ICP-MS results for the major and minor elements reported as oxides (wt %) and standard deviations for the replicated measurements

	Na ₂ O	MgO	Al ₂ O ₃	SiO ₂	K ₂ O	CaO	TiO ₂	MnO	Fe ₂ O ₃	CoO	NiO	CuO	ZnO	As ₂ O ₃	SnO ₂	Sb ₂ O ₅	PbO
PG39	22.4	0.6	0.8	63.2	0.3	11.6	0.08	0.05	0.4	0.00023	0.0009	0.29	0.0018	0.006	0.004	0.0029	0.006
stdev	8.2	0.2	0.4	25.4	0.1	4.5	0.03	0.02	0.2	0.00008	0.0003	0.09	0.0009	0.002	0.001	0.0009	0.002
PG63	17.7	3.6	0.37	68.5	1.9	6.3	0.033	0.023	0.30	0.00040	0.00124	0.46	0.021	0.014	0.059	0.0088	0.0254
stdev	1.6	0.2	0.01	4.1	0.1	0.4	0.001	0.001	0.01	0.00003	0.00008	0.03	0.002	0.001	0.001	0.0004	0.0008
PG84	6.3	1.1	4.1	74.3	4.9	2.9	0.14	0.026	1.7	0.08	0.24	4.3	0.014	0.19	0.044	0.08	0.007
stdev	1.1	0.3	1.3	12.9	0.8	0.5	0.03	0.005	0.5	0.02	0.05	0.8	0.002	0.03	0.007	0.01	0.001
PG87	6.3	0.9	3.1	78.5	4.8	2.2	0.09	0.021	0.9	0.0045	0.010	3.6	0.010	0.0056	0.13	0.0034	0.006
stdev	0.7	0.1	0.3	8.0	0.5	0.2	0.01	0.003	0.1	0.0005	0.001	0.4	0.004	0.0007	0.02	0.0003	0.001
PG89	20.4	0.39	0.41	67.9	0.204	8.0	0.115	0.201	0.36	0.00034	0.00198	1.69	0.0014	0.018	0.0013	0.016	0.083
stdev	0.8	0.02	0.02	3.5	0.006	0.4	0.004	0.006	0.01	0.00002	0.00005	0.04	0.0001	0.001	0.0001	0.001	0.008
PG97	21.4	0.51	0.5	65.4	0.31	9.1	0.08	0.03	0.31	0.00019	0.0014	2.1	0.0014	0.025	0.0034	0.009	0.007
stdev	1.9	0.09	0.1	11.8	0.05	1.5	0.01	0.01	0.07	0.00006	0.0002	0.4	0.0002	0.007	0.0007	0.001	0.002
PG109	15.3	1.3	2.6	72.6	0.25	5.5	0.049	0.9	0.45	0.020	0.021	0.33	0.013	0.0008	0.0026	0.21	0.0101
stdev	1.2	0.2	0.3	6.2	0.01	0.5	0.005	0.1	0.06	0.002	0.002	0.03	0.001	0.0001	0.0006	0.01	0.0007
PG110_1	19.4	0.7	0.7	71.7	0.28	4.9	0.08	1.5	0.4	0.0005	0.0008	0.24	0.0020	0.0015	0.0029	0.006	0.007
stdev	5.7	0.2	0.2	20.5	0.08	1.5	0.02	0.6	0.1	0.0002	0.0002	0.07	0.0006	0.0005	0.0009	0.003	0.002
PG111	20.7	2.8	4.8	66.0	0.17	2.9	0.048	0.50	0.61	0.025	0.035	0.19	0.021	0.0017	0.001344	0.38	0.00085
stdev	2.1	0.3	0.5	6.6	0.02	0.3	0.005	0.05	0.07	0.003	0.004	0.02	0.002	0.0002	0.000003	0.04	0.00003
PG112	14.5	0.7	0.9	75.3	0.29	5.6	0.09	1.36	0.4	0.0006	0.0008	0.7	0.0023	0.0023	0.004	0.007	0.013
stdev	3.1	0.1	0.2	17.4	0.06	1.1	0.02	0.29	0.1	0.0002	0.0003	0.2	0.0006	0.0006	0.001	0.001	0.004
PG116	18.9	0.50	0.30	73.7	0.238	4.8	0.033	0.58	0.23	0.0007	0.0010	0.61	0.0016	0.0019	0.0073	0.0021	0.014
stdev	0.3	0.03	0.02	1.5	0.007	0.1	0.001	0.01	0.01	0.0002	0.0002	0.01	0.0003	0.0001	0.0001	0.0007	0.001
PG121	20.2	3.3	2.5	64.0	2.0	5.6	0.16	0.028	1.1	0.0007	0.0069	0.64	0.006	0.0025	0.00022	0.013	0.014
stdev	2.5	0.5	0.3	8.1	0.2	0.7	0.02	0.004	0.1	0.0001	0.0008	0.08	0.001	0.0004	0.00004	0.003	0.005
PG122	21.6	3.9	3.1	57.8	1.5	7.8	0.25	0.04	1.5	0.0009	0.0071	1.6	0.061	0.0011	0.0002	0.08	0.005
stdev	5.0	0.5	0.4	8.2	0.4	1.1	0.03	0.01	0.2	0.0001	0.0009	0.2	0.006	0.0004	0.0001	0.01	0.003
PG158	5.6	0.8	1.8	79.7	7.0	2.8	0.060	0.018	1.0	0.15	0.28	1.1	0.051	0.26	0.027	0.21	0.10
stdev	0.7	0.1	0.3	12.0	0.9	0.4	0.009	0.002	0.1	0.02	0.03	0.2	0.006	0.03	0.003	0.03	0.01
PG159	6.8	1.36	5.5	74.7	5.4	3.4	0.180	0.038	1.98	0.194	0.271	0.57	0.0113	0.172	0.025	0.0109	0.0024
stdev	0.2	0.05	0.1	3.6	0.3	0.1	0.005	0.001	0.07	0.004	0.005	0.02	0.0005	0.005	0.002	0.0006	0.0003
VG22	6.2	0.8	2.1	77.1	10.4	3.3	0.070	0.018	0.9	0.12	0.18	0.15	0.026	0.055	0.0013	0.073	0.058
stdev	0.5	0.1	0.3	10.0	1.3	0.5	0.008	0.003	0.1	0.01	0.02	0.05	0.002	0.005	0.0001	0.008	0.006
VG106	18.9	2.4	5.3	66.7	0.11	4.5	0.036	0.46	0.73	0.081	0.057	0.002	0.066	0.00022	0.00004	0.0031	0.0010
stdev	1.6	0.2	0.4	5.6	0.01	0.4	0.003	0.04	0.07	0.007	0.005	0.002	0.006	0.00002	0.00001	0.0008	0.0004

Table 5 LA-ICP-MS results for the trace elements (expressed in ppm) and standard deviations of the replicated measurements

	V	Rb	Sr	Zr	Cs	Ba	La	Ce	NdD	Sm	Eu	Gd	Tb	Dy	Er	Yb	Lu	Hf	Ti	Th	U
PG39	10.1	8.4	407.9	105.7	0.22	71.1	5.0	8.1	4.7	0.9	0.24	1.0	0.14	0.9	0.5	0.5	0.08	2.1	0.01	0.8	2.8
stdev	4.5	3.7	159.4	40.2	0.08	26.4	2.1	3.3	2.0	0.3	0.07	0.4	0.05	0.3	0.2	0.2	0.04	0.8	0.01	0.4	1.2
PG63	5.4	10.7	449.7	n.d.	0.32	42.9	1.7	3.7	1.36	0.27	0.07	0.28	0.036	0.23	0.13	0.12	0.019	0.15	0.04	0.3	0.14
stdev	0.3	0.3	26.1	-	0.03	0.7	0.2	0.8	0.08	0.05	0.01	0.02	0.007	0.05	0.01	0.04	0.003	0.03	0.02	0.1	0.03
PG84	24.2	119.7	168.2	n.d.	1.0	101.5	6.3	12.9	6.0	1.3	0.3	1.3	0.18	1.1	0.7	0.7	0.09	1.0	0.011	2.6	0.6
stdev	4.2	22.9	30.8	-	0.2	19.5	1.1	2.6	1.2	0.3	0.1	0.2	0.03	0.2	0.2	0.2	0.02	0.2	0.002	0.6	0.1
PG87	15.7	90.1	128.7	n.d.	0.8	91.8	5.1	10.8	4.6	1.0	0.20	0.99	0.14	0.9	0.50	0.52	0.08	0.85	0.05	2.0	0.56
stdev	1.9	9.6	13.3	-	0.1	12.6	0.3	1.5	0.6	0.1	0.02	0.08	0.02	0.1	0.06	0.03	0.01	0.09	0.01	0.2	0.06
PG89	10.9	4.4	297.8	280.1	0.4	51.3	4.7	7.0	4.3	1.0	0.18	0.84	0.1262	0.77	0.49	0.58	0.09	6.36	0.038	0.82	1.3
stdev	0.7	0.3	13.1	11.6	0.1	1.7	0.1	0.4	0.2	0.1	0.04	0.07	0.0008	0.09	0.06	0.07	0.02	0.09	0.007	0.03	0.1
PG97	7.9	25.3	391.9	106.9	0.5	54.5	4.8	7.7	4.5	0.9	0.20	0.9	0.104	0.8	0.47	0.5	0.07	2.3	0.06	0.8	2.8
stdev	1.6	4.3	65.7	18.5	0.1	10.1	0.7	1.4	0.9	0.2	0.06	0.2	0.006	0.1	0.08	0.1	0.02	0.4	0.03	0.2	0.4
PG109	13.1	6.6	183.2	n.d.	0.15	162.7	2.8	7.0	7.5	2.1	0.58	2.5	0.34	1.8	0.9	0.88	0.11	0.80	0.004	0.87	0.84
stdev	0.8	0.5	14.8	-	0.02	14.2	0.2	0.8	0.9	0.2	0.06	0.4	0.04	0.3	0.1	0.08	0.01	0.08	0.002	0.07	0.05
PG110_1	9.2	4.1	180.4	38.6	0.09	255.0	5.4	6.5	4.8	0.9	0.21	1.0	0.13	0.7	0.4	0.4	0.06	1.0	0.038	0.7	0.7
stdev	3.0	1.1	51.8	11.4	0.02	74.6	1.5	1.7	1.4	0.3	0.09	0.3	0.05	0.2	0.1	0.1	0.03	0.3	0.006	0.2	0.2
PG111	11.0	3.4	85.5	n.d.	0.080	59.6	3.6	9.1	7.9	2.5	0.73	3.2	0.42	2.1	0.9	0.71	0.09	0.59	0.01	1.2	1.1
stdev	0.9	0.5	8.6	-	0.004	6.5	0.3	1.1	0.6	0.1	0.09	0.4	0.08	0.3	0.1	0.05	0.02	0.08	0.01	0.2	0.2
PG112	10.4	8.7	241.4	n.d.	0.29	341.5	7.4	10.1	6.7	1.2	0.3	1.2	0.14	1.0	0.47	0.6	0.08	1.2	0.06	1.2	1.0
stdev	2.6	1.8	50.7	-	0.06	74.8	1.9	2.6	1.6	0.7	0.1	0.1	0.04	0.4	0.05	0.2	0.06	0.1	0.03	0.4	0.4
PG116	8.8	2.4	208.9	31.1	0.077	110.8	1.51	2.69	1.46	0.31	0.062	0.38	0.051	0.25	0.17	0.202	0.031	0.70	0.01	0.31	0.48
stdev	0.2	0.2	2.5	0.5	0.003	0.5	0.06	0.04	0.06	0.03	0.005	0.07	0.005	0.02	0.03	0.006	0.008	0.07	0.01	0.03	0.02
PG121	17.5	15.1	174.5	44.8	0.23	46.6	8.9	19.3	9.0	2.0	0.39	1.8	0.25	1.5	0.9	0.8	0.12	1.3	0.005	2.9	0.51
stdev	2.2	1.5	23.8	6.0	0.02	6.0	1.2	2.4	1.2	0.3	0.04	0.2	0.05	0.3	0.1	0.1	0.01	0.2	0.004	0.4	0.07
PG122	23.4	14.8	216.0	n.d.	0.26	73.4	10.2	21.3	9.6	2.0	0.42	1.8	0.26	1.6	0.9	0.8	0.12	1.4	0.006	3.3	0.6
stdev	3.3	3.4	29.2	-	0.08	11.2	1.4	3.0	1.5	0.3	0.08	0.3	0.03	0.2	0.1	0.1	0.02	0.2	0.004	0.5	0.1
PG158	11.1	164.0	160.1	n.d.	0.6	68.4	3.5	7.4	3.2	0.7	0.16	0.62	0.09	0.58	0.34	0.34	0.04	0.54	0.025	1.2	0.28
stdev	1.5	23.1	23.3	-	0.1	10.8	0.5	1.3	0.6	0.1	0.01	0.02	0.02	0.07	0.05	0.09	0.01	0.08	0.006	0.2	0.06
PG159	38.5	118.7	195.7	n.d.	1.13	156.0	8.7	18.4	8.9	1.93	0.43	1.80	0.26	1.69	0.92	0.98	0.13	1.3	0.035	3.0	0.79
stdev	0.8	6.0	3.9	-	0.08	4.0	0.1	0.6	0.3	0.09	0.04	0.08	0.02	0.05	0.08	0.06	0.01	0.1	0.004	0.1	0.05
VG22	13.4	131.7	173.2	20.7	0.60	75.7	3.9	8.1	3.6	0.7	0.17	0.8	0.11	0.7	0.43	0.4	0.06	0.6	0.021	1.5	0.32
stdev	1.8	20.7	22.3	2.9	0.05	10.8	0.5	0.5	0.4	0.1	0.03	0.1	0.01	0.1	0.08	0.1	0.01	0.1	0.006	0.2	0.02
VG106	5.9	1.5	171.6	16.6	0.060	36.5	2.1	7.6	9.1	3.3	1.04	4.8	0.58	3.4	1.38	1.0	0.13	0.34	0.006	0.76	0.5
stdev	0.4	0.2	13.3	1.4	0.006	2.8	0.1	0.8	0.8	0.1	0.09	0.6	0.07	0.2	0.05	0.1	0.01	0.07	0.005	0.07	0.1

n.d.: not determined

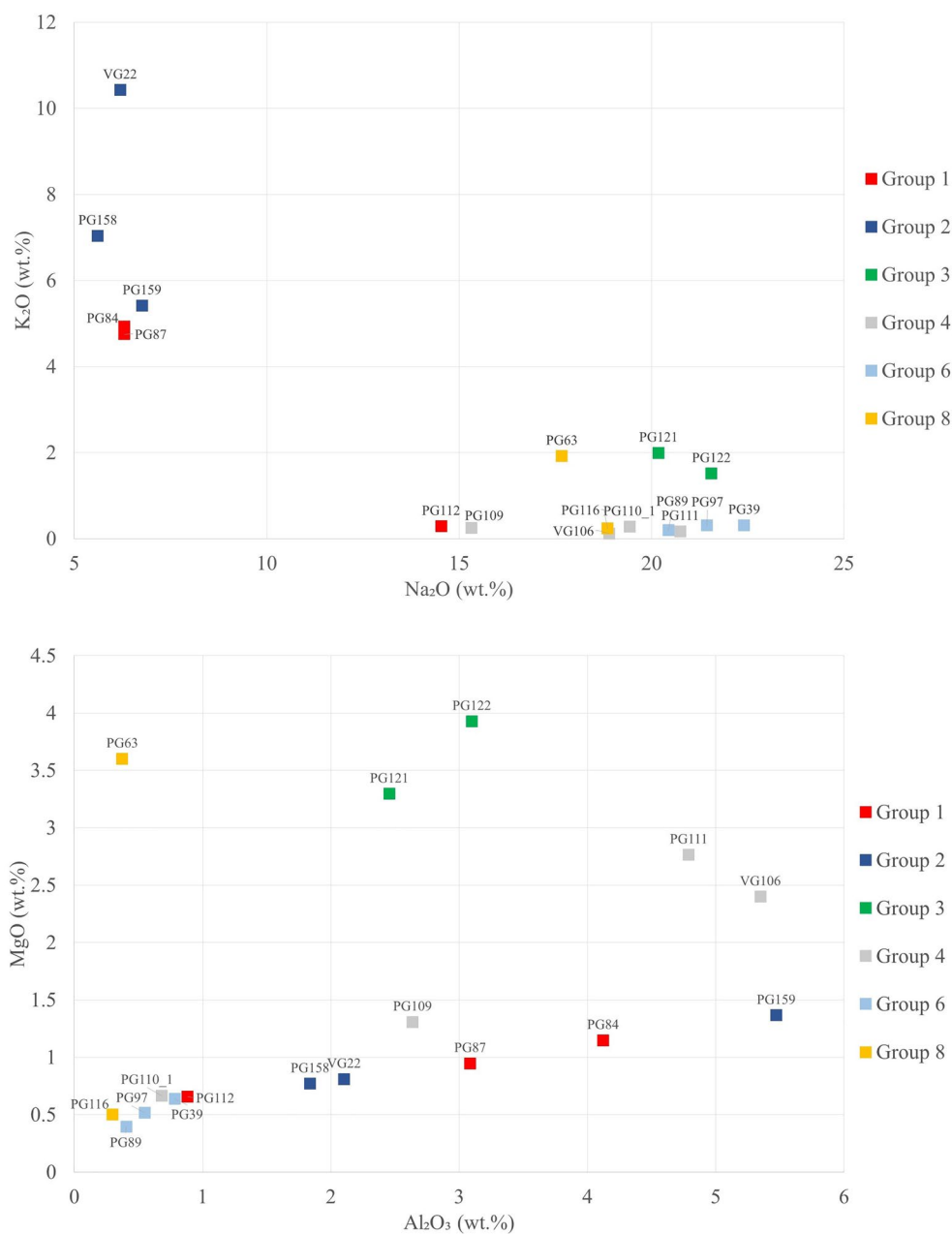


Fig. 9 LA-ICP-MS results. Binary plot of Na₂O vs K₂O (top) and Al₂O₃ vs MgO (bottom)

Data for REE normalised to the Upper Continental Crust (values from McLennan [67]) and several other trace elements (Hf, Th, and U) are reported in Fig. 10. They suggested other kinds of subdivision, beside those emerging from the major elements. Samples of groups 1 and 2 followed a similar pattern (except PG112), with PG159 having higher REE values (Fig. 10, top). Group 4 featured high levels of Eu, Tb, and Dy, followed by the

samples of Group 3 and PG159 from Group 2. Nevertheless, the general profile of the samples of Group 3 was flatter along the considered elements. PG110_1, and PG112 showed negative Ce anomaly (Fig. 10). In Group 6, samples featured high Hf relative concentrations. The trend for Group 8 samples, with levelled profiles, was similar to those of Groups 1, 2 and 3, though the relative concentration of REE differed for each group (Fig. 10). U and Th values kept together some

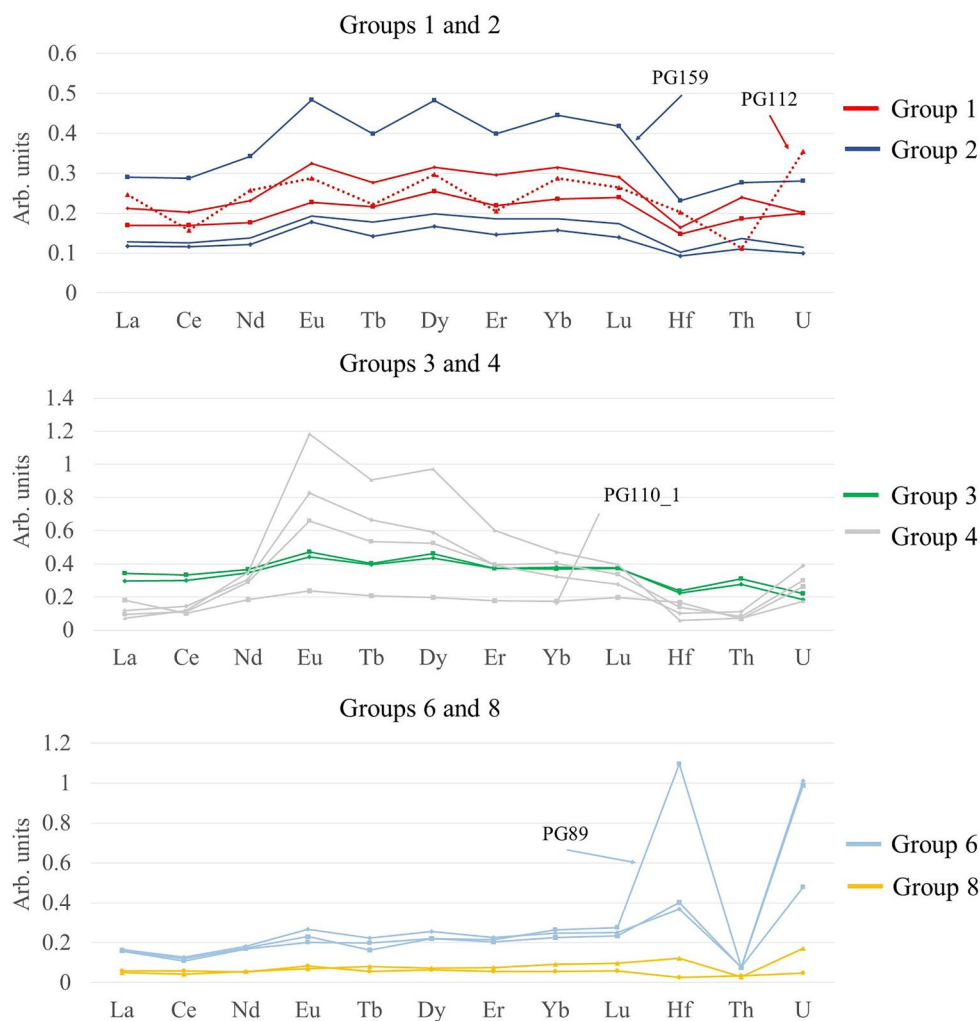


Fig. 10 REE values plus Hf, Ti, Th and U normalised to Upper Continental Crust values (McLennan, 2001)

samples despite their different typology: Groups 4 and 6 (plus PG112 and 116 from Groups 1 and 8 respectively) showed U prevailing over Th, whereas the normalized values for these two elements were similar in the rest of the samples.

Discussion

The data reported in Sect. "Results" are discussed in this section keeping the same typological frame presented in 2.1, with the aim to infer some conclusions about the sources of silica, the type of flux, the colourants and the opacifiers used in the blue-green base glass and in the white and yellow decorations. The compositional data reported in the previous section highlighted some heterogeneity within the sample set, therefore the attention is focussed both on every typological group separately (and in some instances on one sample individually) and

also on the overall set of samples, in order to highlight any specific aspect that can contribute new knowledge on the glass circulating in IE central Italy.

Silica sources

The chemical composition of sand (or of the silica source that was used in glassmaking) can trace the provenance of the primary glass. To properly discuss the compositional data of the glass in order to draw some conclusion on the silica source, we need to pick out those elements that would enter the batch exclusively with the network former [68]. In the present case, due to the variety of colourants used for the glass, the following set of elements was selected to investigate the silica source: Ti, V, Zr, REE, Hf, Th and, partially, U. The latter one can also enter the batch through natural evaporites employed as fluxes and therefore should be reconsidered after the overall discussion of the data [66].

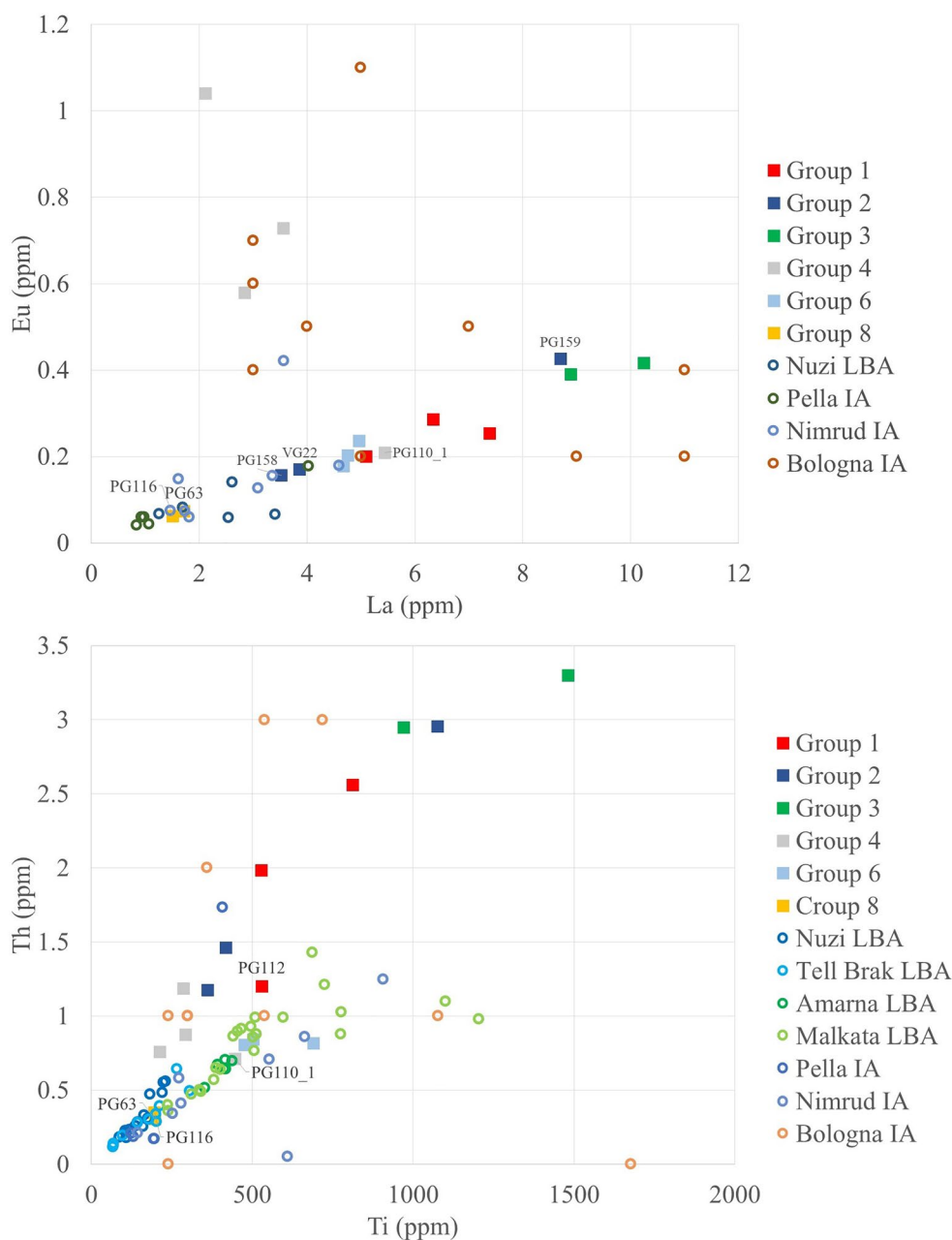


Fig. 11 LA-ICP-MS data obtained in this work for some chemical elements reasonably related to the source of silica, compared with some published data. La vs Eu (top), Ti vs Th (bottom). External data refers to glass from: Nuzi LBA, Tell Brak LBA, Amarna LBA, Malkata LBA – [69]; Bologna IA – [70]; Pella IA and Nimrud IA – [71]

LA-ICP-MS results highlighted, for samples of Group 4, a higher content of Eu, Tb, and Dy in comparison to other REE. The La vs. Eu binary plot (Fig. 11, top) demonstrated the trend in greater detail. Indeed, Group 4 samples (except PG110_1) followed a different trend line, which might be an indicator of separate provenance, possibly Mesopotamia, as they fit the trend of the glasses from Bologna (imported from Mesopotamia) and

Nimrud [70, 71]. On the other hand, the enrichment in middle-REE might be a consequence of the addition of an Egyptian source of cobalt. This evidence, together with the low content of K₂O (Fig. 9, top) indicated as an alternative hypothesis that these samples could be associated with Egyptian production.

Another difference occurred for Hf values for several samples of Group 6. Hf is commonly associated with

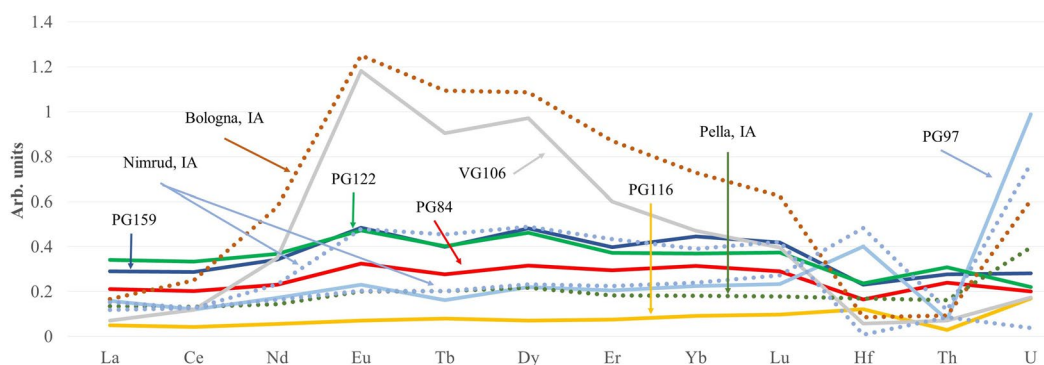


Fig. 12 REE + Hf, Th and U linear plot of UCC normalised values (one sample per group). External data sources (dotted lines): Bologna IA – [70]; Pella IA and Nimrud IA – [71]

Zr in sands as an indicator of heavy mineral impurities [66, 72], and the ratio of heavy minerals was used as a proxy for glass provenance in many case-studies [73–75]. Although Zr was not included in our element list, we may reasonably assume that Hf would mirror its trend. High Hf glasses from Group 6 contained 3.6 ppm of Hf on average, while the mean value for the rest of the samples is 0.8, i.e. 4.5 times less. High Zr content is typical for glass made from Egyptian sands [69], therefore Egypt could be the possible origin for these samples. It is worth stressing that the peculiar Hf content of some samples from Group 6 was associated with the higher Ti/Fe ratio – 0.18 against an average of 0.09 – calculated across all the groups. This evidence might not necessarily point to a different provenance, as it could also derive from the intentional selection of sands of a specific colour—thus different amount of Fe in comparison to Ti to obtain the desired colour of the resulting glass.

Samples of Groups 1, 2 and 3 followed a same line in the Ti vs Th plot in Fig. 11 (bottom). They share this trend with other glasses found in Iron Age contexts on the Italian peninsula, and to a lesser extent with samples of Group 4. It seems that all these glasses were made with sands that derived from similar parental rocks, but despite the different Ti/Th ratio, no other compositional clues emerged to distinguish them from other Mediterranean glasses. Samples from Groups 1, 2 and 3 usually featured the highest concentrations of REE (as shown in Fig. 12), with Group 4 representatives featuring the highest concentrations of middle-REE. Sands used to produce glasses of Group 3 seem to be even richer in impurities than that employed for groups 1 and 2, although all these groups demonstrated similar profiles with a slightly negative Hf anomaly. Group 4 glasses should be associated with Group 1, 2 and 3 samples, but with less Ti.

By considering the overall data, we can suggest that the glasses considered in this study were made by three

or, perhaps, even four different kinds of sand. This might signify three or four different sites of production: glass of the beads of Groups 1, 2 and 3 was made with sands richer in REE impurities (except PG112); Group 4 samples (except 110_1) featured distinctly higher Eu, Tb and Dy relative concentrations, which would point to separate provenance, although also some colouring raw materials could contribute to these elements to the batch; Groups 5 and 6 were made of sands with higher Zr content, whereas the glass of the beads belonging to Groups 7 and 8 was made from relatively pure silica. The origin of the glass of Groups 4 to 8 would be Mesopotamian, though higher Ti and Hf content were more inherent to the glasses of Egyptian origin [69].

Fluxes

Alkali-rich substances such as soda evaporitic deposits or halophytic plant ashes were used as fluxes for glass production in the Iron Age Mediterranean [76]. Alkali and alkali-earth element concentrations play a key role in distinguishing the source of the fluxing components in the glass batch. Figure 13 shows the division that emerged between the groups with high K_2O values and those with high MgO. The general criterion to recognize mineral-flux glass (produced with the addition of Egyptian natron or similar evaporitic deposit) is the content of both K_2O and MgO lower than 1.5% [77–80]. Groups 4, 6 and 8 (except PG63), plus PG112 from Group 1 fitted this criterion. Figure 10 shows that U level, which is also an indicator of the mineral flux, was higher than the Th one in these glasses.

PG63 (this sample represents also Group 7, PG33 and PG170 analysed with p-XRF that produced similar results for K) and the samples of Group 3 clustered together and separated from the other samples with high Na_2O . On the other hand, high K_2O concentrations in the samples

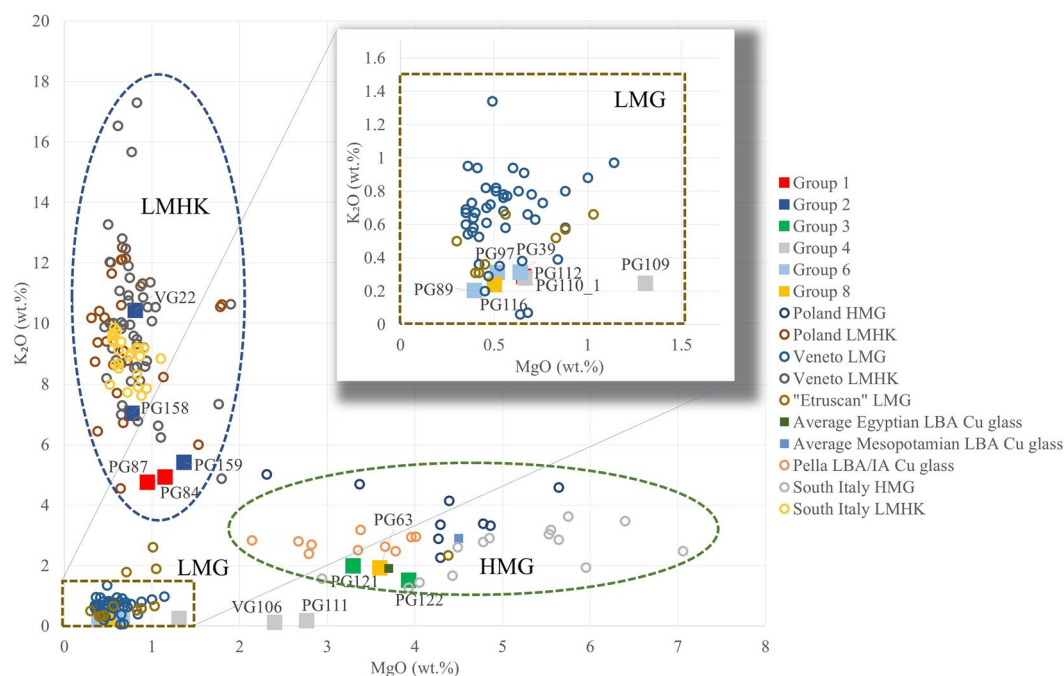


Fig. 13 MgO vs K_2O plot. Groups 1–8 are representatives for samples considered in the present study. External data sources: Poland HMG and Poland LMHK – [5]; Veneto LMG and Veneto LMHK – [4]; “Etruscan” LMG – [82]; Average Egyptian and Mesopotamian LBA Cu glass – [83]; Pella LBA/IA Cu glass – [71]; South Italy HMG and LMHK glass – [84]

of Groups 1, 2 and 3 were the evidence of plant ash used as a flux to make these glasses.

Samples of the present study were compared with several flux-determined compositional groups of glasses from the Bronze and the Iron Ages. The LMHK group of samples represented by the values of glasses found in Poland, South Italy and Veneto (North Italy) was associated with the LBA glass-making site of Frattesina [4, 8, 81].

Fluxing material for this type of glass could be potassium-rich plant ash with low content of magnesium and calcium, although we cannot establish the species of the plants that were burned or the technological processes of the ash preparation due to the high variability of the resulting ash composition [1, 81]. Groups 1 and 2 samples (without PG112 and PG169) fitted this glass composition.

Group 3, PG63, 169 and, incidentally, Group 7 (based on XRF data) fell in the range for HMG, therefore soda-rich ash was employed as a flux to produce the glass of these beads.

Higher Mg concentrations in the glasses of Group 4 can be explained by the cobalt-bearing alum that was a popular choice of cobalt ore, as discussed in “Colourants and opacifiers” Sect. Taking into consideration the contribution of the colourant, the composition of these samples could be placed in the LMG interval, along with

Groups 6 and 8 (without PG63), with natron used as the fluxing agent.

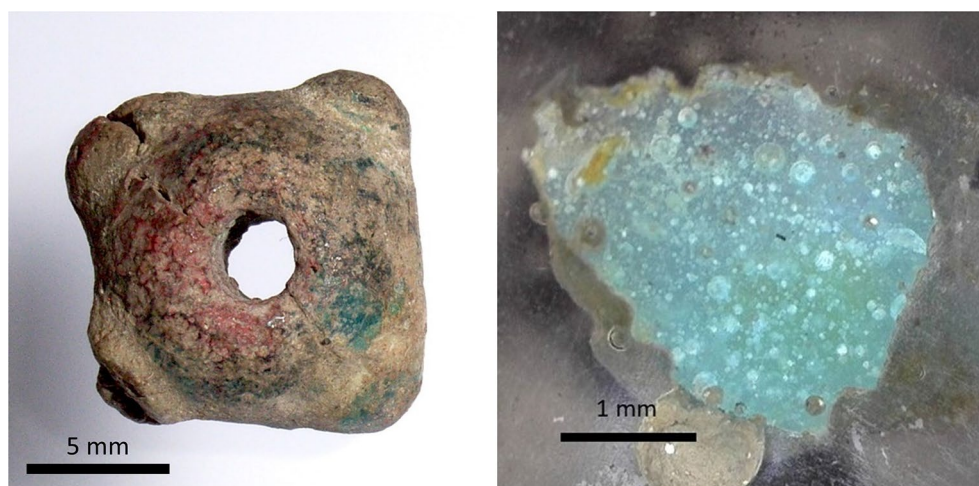
Colourants and opacifiers

Details on the information that was obtained from the different analytical approaches are reported in Table 6.

In several cases, the typological groups included samples of various colour. All the samples of Group 1, despite the difference in their appearance (Fig. 2), owe their colours to copper. As already mentioned in “Fibre Optics Reflection Spectroscopy (FORS)” Sect., all the red glasses were coloured in the same way as VG24 (Group 2), i.e. with metallic copper particles suspended in the glass matrix. VG25 shows a peculiar situation, featuring both red and green–blue parts without specific boundaries (Fig. 14, left). Other samples, probably from the same necklace, had similar spots of dark and dark-blue colour. Since the red colouring with Cu^0 requires precise redox conditions of the furnace and cooling process, it can be suggested that either these conditions were not kept perfectly, resulting in some copper dissolving in the matrix in octahedral coordination with non-bridging oxygen atoms, or firing of the beads occurred, possibly during the funerary rituals. Evidence supporting the first hypothesis was found in Frattesina: a piece of the crucible covered in green–blue glass with opaque red glass whirls [4]. A bead discussed in Angelini et al. [85] has distinct

Table 6 Information on chromophores and opacifiers with the indication of the methods that provided the information

	Samples	Chromophore(s)/Opacifier	Technique for confirmation
RED	VG24, 25, 26, 29	Cu^0	FORS, p-XRF
GREEN	PG65, 121, 122, 160, 161, 166, 169	Cu^{2+} , Fe^{3+}	FORS, p-XRF, LA-ICP-MS
DARK-GREEN	PG84, 87, 162, 163, 164, 167, VG25	Cu^{2+} , Fe^{3+}	FORS, p-XRF, LA-ICP-MS
BLUE-GREEN	PG110_1, PG112	Cu^{2+} , Fe^{3+}	FORS, p-XRF, LA-ICP-MS
BLUE	PG33, 39, 59, 60, 63, 88, 89, 97, 116, 136, 170, VG28	Cu^{2+} , Fe^{3+}	FORS, p-XRF, LA-ICP-MS
Co–Cu BLUE	PG109, 111, 138, VG106	Co^{2+} , Cu^{2+} , Fe^{3+} , Fe^{2+}	FORS, p-XRF, LA-ICP-MS
Co BLUE	PG168, 171	Co^{2+} , Fe^{3+} , Fe^{2+}	FORS, p-XRF
DARK	PG158, 159, VG22, 23	Co^{2+} , Fe^{2+} , Fe^{3+}	FORS, p-XRF, LA-ICP-MS
WHITE 1	PG109, 110_1, 111, 112, 138, 170, VG 106	CaSb_2O_6	p-XRF, SEM–EDS, μ -Raman, LA-ICP-MS
WHITE 2	PG84, 167, VG25, 26, 29	Fine bubbles	OM, p-XRF, μ -Raman, LA-ICP-MS
YELLOW	PG59, 60, 122, 166	$\text{Pb}_2\text{Sb}_2\text{O}_7$	p-XRF, μ -Raman, LA-ICP-MS

**Fig. 14** Sample VG25 (left, photograph presented by the concession of the Museo Nazionale Etrusco di Villa Giulia). Differently coloured parts can be observed. Sample PG121 (right) cross-section. Bubbles on and beneath the surface can be observed

zones of blue and red colour that have defined boundaries, with metallic copper crystals 2–4 microns in size observed by transmission electron microscopy in the red parts. On the other hand, another source of the red colour would be the burial practice of cremation, which was the case for the tomb where the samples considered in this study were found. Reducing flames must have heated the bead causing the alteration of the surface without softening the glass.

In addition, all the green–blue coloured samples of Group 1 (PG84, 87, 112, 167 and 169) had high values of copper (>0.7% CuO). FORS spectra proved the already mentioned Cu^{2+} presence, which is obtained by heating the glass in an oxidising environment. Co was also detected in PG84 by p-XRF and LA-ICP-MS, but FORS spectra demonstrated that it did not affect the colour, probably because of its oxidised redox state. Different

workshops in Po valley and north of the Alps that might have produced LMHK glass seemed to be specialised in the use of specific colourants (Cu and Co), as suggested by Towle and considered in Koch [26], but it was impossible to assign Group 1 and 2 samples to a specific workshop based on their Cu and Co concentrations. A greenish tinge might be created by the Fe^{3+} , as its absorption modifies the spectrum of Cu-coloured glass shifting the maximum of reflectance towards the red region, which resulted in the greenish hue of the Cu^{2+} – Fe^{3+} glass.

Group 2 samples (Vulci ring beads) are dark (VG22, 23) or red (VG24). FORS spectra for VG23 demonstrated Fe^{3+} , Fe^{2+} , and Co^{2+} bands, while spectra for VG24 revealed Cu^0 and Fe^{2+} ; this latter was expected because Fe, and also Sb, act as reducing agents to promote the formation of metallic copper micro-particles [86]. p-XRF

analyses detected in fact both Fe_2O_3 (0.72%), and Sb_2O_5 (0.21%). VG22, 23, PG158 and 159 were coloured by cobalt, which was present in all the beads of Group 2 (including VG24, in the lowest amount, but excluding PG161). Co was confirmed by both p-XRF (all samples) and LA-ICP-MS (for those analysed with this technique). Fe (either in the oxidised or in the reduced form) might also influence the colour of all the samples in this group, in addition to Co^{2+} , which is the main chromophore. PG161 was Cu-coloured (Fig. 3) with Sn also detected by the p-XRF.

The green colour of the bodies of Group 3 is caused by the presence of Cu^{2+} and Fe^{3+} (evident from FORS spectra and confirmed on elemental bases by p-XRF). The p-XRF analyses also revealed the presence of Sb and Pb in minor quantities in some of the samples (less than 0.3% of each oxide in PG166, LOQ bordering values in PG65, and PG160), although these elements could derive from the partial inclusion of the decoration in the analytical spot of the p-XRF, as they were not detected by LA-ICP-MS in the bulk bodies of PG121 and PG122. Since no compositional evidence of opacification emerged, it was concluded that the small bubbles observed under the optical microscope (Fig. 14 right) in the glass matrix were the cause of the opaque appearance.

The colour of Group 4 was already discussed in a preliminary paper [34], and data from the micro-invasive approach presented here gave a further insight into the composition of these beads. The Cu content determined by p-XRF in VG106 was not confirmed by LA-ICP-MS, placing that bead into the Co-coloured group [34]. For the rest of the samples, LA-ICP-MS indicated that PG110_1 and PG112 (which were preliminarily assigned to the Co–Cu coloured group) appear to be solely coloured by Cu^{2+} , as no Co was detected. PG109 and PG111 featured Cu and Mn in comparable concentrations, with also 200–250 ppm of CoO – a concentration sufficient to influence the colour, but too low to justify the inclusion of this bead into the Co-coloured beads group highlighted in [34], which featured some 400–900 ppm Co according to p-XRF data.

Group 5 and 6 samples appear to be Fe–Cu coloured, a configuration that was closer to PG110_1 and PG112 samples. Fibula bow beads (Group 7) also have Cu^{2+} as the main colourant.

Group 8, which includes differently coloured beads, showed data that proved a Cu^{2+} colouration for most of the samples. Two exceptions were PG168 and 171, which were coloured by Co^{2+} , Fe^{2+} and Fe^{3+} . The opaque bead PG170 probably had calcium antimonate crystals suspended in the matrix in addition to dissolved Cu^{2+} , as p-XRF analysis detected 2.6% of Sb_2O_5 and one of the highest CaO concentrations in Group 8 (7.2%).

Regarding the decorations, samples of Group 1 show no compositional evidence of white opacifiers but PG112, which might contain CaSb_2O_6 in its white part, which was also detected through Raman in all the samples of Group 4. Apatite, as a white opacifier, already proposed by Towle and Henderson [82] for “Etruscan” glasses was excluded for PG84 (Group 1) since no significant P peaks were present in any of the p-XRF spectra. Low and scattered P counts were obtained for PG84 analysis with LA-ICP-MS; although the high concentration of Ca detected by p-XRF in the white decoration of a reddish subgroup of samples (namely, VG25, 26 and 29) would not exclude its presence in these samples. Given the rough surface, which was comparable with those observed for Group 3 samples, we could also assume that the opaque white appearance was caused by the bubbles densely distributed in the colourless glass.

Yellow decorations of Groups 3 and 7 owed their appearance to lead antimonate – $\text{Pb}_2\text{Sb}_2\text{O}_7$, confirmed by the Raman analysis, which further supported the elemental compositional evidence.

Dark-coloured decorations in Group 3 samples did not show any significant compositional difference from the main bodies, except for some lower (if any) concentrations of Fe and Cu. Therefore, it is still unclear what agent was responsible for dark colouration.

As bronze could be the source of copper in the samples, the quantitative relationship between copper and tin was investigated. p-XRF data for samples in which both Cu and Sn were detected show a weak positive correlation ($r=0.61$). A positive relationship also emerges from LA-ICP-MS data. The average ratio of Sn and Cu in ancient bronzes is typically assumed to be 1:10 [83], but low tin bronzes were also produced for specific purposes in the Bronze and, later, in the Iron Age Mediterranean [87, 88]. Here, the average value for this ratio was 0.025, which excluded bronze as the source of copper, except for PG63, for which this ratio was 0.13.

Cobalt was associated with Ni, Zn, Fe, Al and Mg in the samples of Group 4. Particularly Co, Ni, and Zn values were roughly equal, while Co was slightly prevailing. This was an indication of the use of Egyptian alum as the raw material for Co [89]. Samples from Group 2 and PG84 featured high Co values, too. For these beads, the lack of Co correlation with Al and Zn, and its strong association with Ni and As (r values 0.87 and 0.65, respectively) made this group of samples similar to the ones from LBA Frattesina, for which a European source of Co was suggested [4].

Conclusion

The scientific investigation of several typological groups of glass beads from Iron Age contexts of Central Italy enabled an insight into the chemical composition of ancient glasses down to trace elements, improved the picture given by the typological classification to face specific archaeological questions and contributed some new knowledge on glass found in IA Central Italy.

First of all, it emerged that beads from Group 1 (except PG112 and 169) and Group 2 probably belong to the Final Bronze Age production that was flourishing in the lower Po valley, supporting the typological attribution with compositional evidence, as they were recognized as LMHK glass. This confirmed the archaeological assumption that beads of FBA glass continued being used also in EIA. Since there is no evidence that the production of LMHK glass continued in the Iron Age, we can assume that these objects were finally put in a grave some 100–150 years after their production. PG112 (Group 1) was an exception, as it could be linked compositionally to another small translucent green–blue bead – PG110_1 (Group 4), with a common (probably Mesopotamian) provenance. Despite the typological attribution to FBA, the flux source for PG112 points to an EIA production, supporting the hypothesis that it could be an imitation of an older local production which, in turn, supported the hypothesis of local glass-working in IA Central Italy.

The chemical composition of the beads in Group 3 kept these samples somehow apart from all the other beads considered here, although some compositional similarities emerged with Groups 1 and 2 for trace elements. As Group 1 and 2 were probably produced locally, this similarity could be suggestive of a local primary production of glass in EIA Central Italy. This assumption remains tentative in the absence of more data, but having determined the composition of these beads gives a first contribution to this topic. The analyses have shown that the two types of beads in Group 3, made of visually similar glass, were also compositionally similar, and sample PG169 was also associated with these samples.

Two hypothesis can be suggested for most of the glass of the beads of Group 4 (since PG110_1 and PG112 made a separate group): provenance could be Egypt according to the evidence of the use of Egyptian Co source and natron as a flux; in addition, the production in Assyrian Nimrud could be suggested for all the cobalt blue beads of the same appearance. Cu (associated with Mn) might have been added to achieve a similar colour.

Groups 5 and 6 glasses probably had a common origin in Egypt (Fig. 12 for Group 6 and Fig. 4 to compare similarly located Groups 5 and 6). These samples, as a rule, have high Hf (and Zr) concentration, and the sand might

have been intentionally selected to contain the proper iron concentration to obtain a specific glass colour. Sample PG136 was re-assigned to Group 6 based on its composition, as this small fragment was only tentatively assigned to Group 8 based on colour and translucency.

Form and distribution indicated that the fibula bow beads (Group 7) were shaped in Central Italy, and we demonstrated here that they were compositionally similar to PG63 glass, with trace element pattern similar to those of the glasses from Nimrud and Pella. The glass was then imported and shaped locally.

For most of the samples of Group 8, compositional data gave no clear suggestions for raw glass provenance, although they can be recognized as imported glass due to the use of natron as the fluxing agent and REE profiles similar to other Eastern Mediterranean glasses.

The colours of glasses in this set were manipulated with the knowledge of the influence of the redox state of the furnace on the final colour of the glass, using Cu, Co, and Fe as the colouring agents. Peculiar was the use of bubbles (intentional or not) for opacification.

In general, the set of beads considered in this work reflected the tendencies of the glass circulation already highlighted for the EIA in the Mediterranean area and beyond – with the transition to the evaporitic deposits as flux, and the simultaneous use, if not local production, of plant ash glass. It appears that the glass supply in Central Italy was divided between the glass imported from the Near East (seemingly both Egypt and Mesopotamia) and small local production of primary glass that grew without continuation with LMHK tradition. Evidence of local working of imported glass also emerged by combining the archaeometric and the typological evidence.

Abbreviations

BCE	Before the Common Era
CCD	Charge-Coupled Device (detector)
CMOG	Corning Museum of Glass
EIA	Early Iron Age
FBA	Final Bronze Age
FORS	Fibre Optic Reflectance Spectroscopy
FWHM	Full Width at Half Maximum
HMBG	High Magnesium Brown Glass
HMG	High Magnesium Glass
IA	Iron Age
INFN	National Institute of Nuclear Physics (Istituto Nazionale di Fisica Nucleare)
LA-ICP-MS	Laser Ablation – Inductively Coupled Plasma – Mass Spectrometry
LBA	Late Bronze Age
LMG	Low Magnesium Glass
LMHK	Low Magnesium High potassium (K)
LOQ	Limit of Quantification
NIR	Near InfraRed
NIST	National Institute of Standards and Technology
OM	Optical Microscopy
PC	Principal Component

PCA	Principal Component Analysis
p-XRF	portable X-Ray Fluorescence spectrometry
QC	Quality Control
REE	Rare-Earth Elements
RSD	Relative Standard Deviation
SDD	Silicon Drift Detector
UCC	Upper Continental Crust
(VP)-SEM-EDS	(Variable Pressure) – Scanning Electron Microscopy coupled with Energy Dispersive Spectrometry

Supplementary Information

The online version contains supplementary material available at <https://doi.org/10.1186/s40494-023-00952-1>.

Additional file 1: Table S11. Typological features of the beads considered in the study. Table S12. Methods applied to analyse each sample. Table S13. Fibre Optics Reflectance Spectroscopy (FORS) results for each sample that produced a meaningful spectrum. Table S14. p-XRF compositions of the samples.

Acknowledgements

Authors would like to express their gratitude to the administrations of Museo Nazionale Etrusco di Villa Giulia and Museo delle Civiltà for allowing and facilitating the on site analyses and agreeing to the laboratory study of the objects. Acknowledgement is extended to Tiziana Forleo, Vincent Gardette and Pedro Barrulas, who helped in establishing the analytical procedures for micro-Raman and LA-ICP-MS analyses.

Author contributions

OY: conceptualisation, validation, formal analysis, investigation, writing—original draft, visualisation, funding acquisition; LK: conceptualisation, investigation, writing – review and editing; AG: methodology, formal analysis, resources, writing – review and editing; GF: methodology, formal analysis, resources, writing – review and editing; PD: methodology, validation, formal analysis, writing – review and editing; LCG: methodology, validation, formal analysis, resources, writing—review and editing; AM: methodology, validation, formal analysis, resources, writing—review and editing; SF: validation, resources, data curation, writing – review and editing; AS: validation, resources, data curation, writing – review and editing, supervision; AR: methodology, resources, writing – review and editing; ALG: methodology, resources, writing – review and editing; MF: methodology, formal analysis, resources, writing – review and editing; MM: methodology, formal analysis, resources, writing – review and editing; CI: conceptualisation, investigation, writing – review and editing, supervision; MG: methodology, validation, resources, writing – review and editing, supervision, project administration, funding acquisition. All authors read and approved the final manuscript.

Funding

This project has received funding from the European Union's Horizon 2020 research and innovation program under the Marie Skłodowska-Curie grant agreement No 754511. The contents of this paper are the sole responsibility of the authors and do not necessarily reflect the opinion of the European Union. M. G. and P. D. acknowledge the Fondo Ricerca Locale 2020 funding provided by the Università degli Studi di Torino.

Availability of data and materials

Data that are not explicitly presented in the paper or the supplementary information may be provided on a reasonable request by the corresponding author.

Declarations

Competing interests

The authors have no competing interests as defined by Springer, or other interests that might be perceived to influence the results and/or discussion reported in this paper.

Author details

¹Department of Chemistry, University of Turin, Via Pietro Giuria, 7, 10125 Turin, Italy. ²Institute of Prehistoric Archaeology, University of Cologne, Weyertal 125, 50931 Cologne, Germany. ³National Institute of Nuclear Physics, National Laboratory of Frascati, via Enrico Fermi 40, 00044 Frascati, Rome, Italy. ⁴Arvedi Laboratory of Non-Invasive Diagnostics, CISRI, University of Pavia, Via Bell'Aspa 3, 26100 Cremona, Italy. ⁵Department of Musicology and Cultural Heritage, University of Pavia, Corso Garibaldi 178, 26100 Cremona, Italy. ⁶Department of Chemistry, University of Bari "Aldo Moro", via, Orabona 4, 70126 Bari, Italy. ⁷Laboratorio di Ricerca per la Diagnostica dei Beni Culturali, University of Bari "Aldo Moro", via Orabona 4, 70126 Bari, Italy. ⁸Museo Delle Civiltà, Piazza Guglielmo Marconi 14, 00144 Rome, Italy. ⁹Department of Physics, University of Turin and INFN Branch in Turin, Via Pietro Giuria, 1, 10125 Turin, Italy. ¹⁰Italian National Research Council, Institute of Heritage Science, A.d.R. RM1, Via Salaria km 29.300, 00015 Montelibretti, Rome, Italy. ¹¹Department of Historical Studies, University of Turin, Via Sant'Ottavio, 20, 10124 Turin, Italy.

Received: 20 December 2022 Accepted: 2 May 2023

Published: 18 May 2023

References

- Henderson J. Electron probe microanalysis of mixed-alkali glasses. *Archaeometry*. 1988;30(1):77–91. <https://doi.org/10.1111/j.1475-4754.1988.tb00436.x>.
- Henderson J. Glass production and bronze age Europe. *Antiquity*. 1988;62(236):435–51. <https://doi.org/10.1017/S0003598X00074548>.
- Brill RH. Chemical analyses of some glasses from Frattesina. *J Glass Stud*. 1992;1:11–22.
- Towle A, Gambacurta G, Bellintani P, Henderson J, Frattesina and Adria: report of scientific analysis of early glass from the Veneto. Frattesina and Adria: report of scientific analysis of early glass from the Veneto. In: Serra F. Editor. *Padusa: bollettino del centro polesano di studi storici archeologici ed etnografici: XXXVII*, 2001; 37:1–62.
- Purowski T, Kępa L, Wagner B. Glass on the Amber Road: the chemical composition of glass beads from the Bronze Age in Poland. *Archaeol Anthropol Sci*. 2018;10(6):1283–302. <https://doi.org/10.1007/s12520-016-0443-8>.
- Bellintani P, Vetri di Frattesina All. Caratterizzazione crono-tipologica, archeometria e confronti 310 nell'ambito della tarda età dell Bronzo dell'Europa centro-orientale e del Mediterraneo. *PADUSA Bollettino del Centro*. 2020;31:1:71–118.
- Henderson J, Evans J, Bellintani P, Bietti-Sestieri AM. Production, mixing and provenance of Late Bronze Age mixed alkali glasses from northern Italy: an isotopic approach. *J Archaeol Sci*. 2015;1(55):1–8. <https://doi.org/10.1016/j.jas.2014.12.006>.
- Paynter S, Jackson CM. Investigating Late Bronze age glass beads from Stotfold, Bedfordshire UK. *Heritage*. 2022;5(2):634–45. <https://doi.org/10.3390/heritage5020035>.
- Angelini I, Nicola C, Artioli G. 2012. Materiali vetrosi protostorici della Sardegna: indagini archeometriche e confronto analitico con reperti coevi. In: *Atti della XLIV Riunione Scientifica. La Preistoria e la Protostoria della Sardegna, Cagliari, Barumini, Sassari 23–28 novembre 2009 Vol. III – Comunicazioni Firenze - Ortacesus (CA) 2012:1131–50*.
- Angelini I, Cupitò M, Bettineschi C, Leonardi G, Molin G. Cronologia di vetri protostorici veneti mediante indagini archeometriche. *Atti del convegno „Riflessioni e trasparenze diagnosi e conservazione di opere e manufatti vetrosi”, Bologna: Patron Editore*. 2010:71–86.
- Mildner S. Glasperlen in der Bronzezeit. *Handelsgut und Prestigeobjekt der Pfahlbausiedler*. Ein Vorbericht. *Plattform*. 2016;23/24:80–83.
- Mildner S, Schüssler U, Falkenstein F, Brätz H. Bronzezeitliches "High Magnesium Glass" in Mitteleuropa – Lithium und Bor als Indizien für eine mögliche Herkunft aus Westanatolien. In: Glaser L. Editor. *Archäometrie und Denkmalpflege 2018. Jahrestagung am Deutschen Elektronen-Synchrotron Hamburg 20.-24. März 2018. Hamburg 2018:132–135*.
- Sayre EV, Smith RW. Compositional categories of ancient glass. *Science*. 1961;133(3467):1824–6. <https://doi.org/10.1126/science.133.3467.1824>.
- Polla A, Angelini I, Artioli G, Bellintani P, Dore A. Archaeometric investigation of early iron age glasses from Bologna. In: *Proceedings of the 37th International Symposium on Archaeometry, 13th-16th May 2008*,

- Springer, Berlin, Heidelberg. Siena, Italy 2011; pp. 139–144. https://doi.org/10.1007/978-3-642-14678-7_20.
15. Walton M, Eremin K, Shortland A, Degryse P, Kirk S. Analysis of Late Bronze age glass axes from nippur—a new cobalt colourant. *Archaeometry*. 2012;54(5):835–52. <https://doi.org/10.1111/j.1475-4754.2012.00664.x>.
 16. Rehren Th, Freestone IC. Ancient glass: from kaleidoscope to crystal ball. *J Archaeol Sci*. 2015;56:233–41. <https://doi.org/10.1016/j.jas.2015.02.021>.
 17. Šmit Z, Laharnar B, Turk P. Analysis of prehistoric glass from Slovenia. *J Archaeol Sci Rep*. 2020;29:102114. <https://doi.org/10.1016/j.jasrep.2019.102114>.
 18. Shortland A, Schachner L, Freestone I, Tite M. Natron as a flux in the early vitreous materials industry: sources, beginnings and reasons for decline. *J Archaeol Sci*. 2006;33(4):521–30. <https://doi.org/10.1016/j.jas.2005.09.011>.
 19. Panighello S, Orsega EF, van Elteren JT, Šelih VS. Analysis of polychrome Iron Age glass vessels from Mediterranean I, II and III groups by LA-ICP-MS. *J Archaeol Sci*. 2012;39(9):2945–55. <https://doi.org/10.1016/j.jas.2012.04.043>.
 20. Haevernick ThE. Urnenfelderzeitliche Glasperlen. *Zeitschr Schweiz Arch u Kunstgesch*. 1978;35:145–57.
 21. Bellintani P, Gonzato F. Luxury production. Amber and Glass during the Recent and Final Bronze Age in Northeastern Italy. In: Fotiadis M, Laffineur R, Lolos Y, Vlachopoulos A, Editors *HESPEROS: The Aegean Seen From The West*. Proceedings of the 16th International Aegean Conference, University of Ioannina, (18–21 May 2016). Leuven. 2017:173–84.
 22. Angelini I, Olmeda G. 2018. Archaeometric study of vitreous materials beads. In: Gallay A, Burri-Wyser E, Menna FC, David-Elbiali E. Editors, *Tolochenaz (VD) – La Caroline. Du Mésolithique à l'époque romaine en passant par le néopole du Boiron*. Cahiers d'Archéologie Romande 168 Lausanne. 323–39.
 23. Rychner-Faraggi AM. Hauterive-Champréveyres 9. Métal et parure au Bronze final. *Arch. Neuchateloise* 17 Neuchatel, 1993.
 24. Bellintani P. Le perle in materiale vetroso dall'antica età del Bronzo all'inizio dell'età del Ferro in Italia. Indicatori di scambio su lunga distanza e prime testimonianze di produzione locale. Il vetro in età protostorica in Italia. In: Ciappi S, Larese A, Ubaldi M. Editors. *Atti delle XVI Giornate Nazionali di Studio (Adria, 12–13 maggio 2012)*. Milano: 2014;15–24.
 25. Angelini I. Archaeometry of Bronze Age and Early Iron Age Italian vitreous materials: a review. In: *Proceedings of the 37th International Symposium on Archaeometry, 13th–16th May 2008, Siena, Italy* Springer, Berlin, Heidelberg 2011:17–23. https://doi.org/10.1007/978-3-642-14678-7_3.
 26. Koch LC. Glas und glasartiges Material in Italien zur Bronze- und Früh-eisenzeit—Forschungsstand und Perspektiven. In: Klimscha F, Karlsen HJ, Hansen S, Renn L. Eds. *Vom künstlichen Stein zum durchsichtigen Massenprodukt. Innovationen in der Glastechnik und ihre sozialen Folgen zwischen Bronzezeit*. Berliner Studien zur Antiken Welt Berlin 2021:67–103.
 27. Arancio ML, Moretti Sgubini AM, Pellegrini E. Corredi funerari femminili di rango a Vulci nella prima età del Ferro: il caso della tomba dei bronzetti sardi. *Preistoria e Protostoria in Etruria. L'alba dell'Etruria. Fenomeni di continuità e trasformazione nei secoli XII–VIII aC Ricerche e scavi*. Atti del IX Incontro di studi (Valentano-Pitigliano, 12–14 settembre 2008), Negroni Catacchio, N.[ed.], Milano: Centro di Studi di Preistoria e Archeologia. 2010:169–213.
 28. Koch LC. Die gemusterten Glasperlen und Anhänger Verucchios (Emilia-Romagna, Italien) des 8.–7. Jhs. v. Chr. – Klassifikation und Verwendung. forthcoming.
 29. Purowski T. Bursztynowy rozdziałacz i szklane paciorki odkryte w obiektach kultury łużyckiej w Targowisku, pow. Wielicki. In: Górski J, Editor. *Via Archaeologica. Źródła z badań wykopaliskowych na trasie autostrady A4 w Małopolsce*, Kraków 2014:289–306.
 30. Mildner S. Das älteste echte Glas in Mitteleuropa. *Bayerische Archäologie*. 2019;4:17–9.
 31. Koch LC. Classificazione tipologica delle Perle di Vetro. In: von Eles P, Bentini L, Poli P, Rodriguez E, editors. *Immagini di uomini e di donne dalle necropoli villanoviane di Verucchio*. All'Insegna del Giglio; 2015 Dec 10. on DVD.
 32. Koch LC. Früheisenzeitliches Glas und Glasfunde Mittelitaliens: eine Übersicht von der Villanovazeit bis zum Orientalisante und eine Analyse der Glasperlen als Grabbeigabe des Gräberfeldes Quattro Fontanili in Veji. *Bochumer Forschungen zur Ur- und Frühgeschichtlichen Archäologie* 4. Leidorf; 2011.
 33. Koch LC. Die Glasperlen des 8. und 7. Jhs. v. Chr. aus Verucchios (Emilia-Romagna, Italien) – Die monochromen Perlen und Augenperlen. *Mitteilungen des Deutschen Archäologischen Institutes, Abteilung Rom*. in press.
 34. Yatsuk O, Gorghinian A, Fiocco G, Davit P, Francone S, Serges A, Koch L, Re A, Giudice AL, Ferretti M, Malagodi M, Iaia C, Gulmini M. Ring-eye blue beads in iron age central Italy—preliminary discussion of technology and possible trade connections. *J Archaeol Sci Rep*. 2023;47:103763. <https://doi.org/10.1016/j.jasrep.2022.103763>.
 35. Stern EM. Clockwise and counterclockwise in ancient core-glass. In: *Annales du 13e Congrès de l'Association Internationale pour l'Histoire du Verre*. Pays Bas / 28 août–1 septembre 1995. Lochem: 1996; 21–32.
 36. Koch LC. Die schwarzen Perlen in Osteria dell'Osa (Rom, Italien): Ein Beitrag zu den ersten Glasperlen der frühen Eisenzeit in Latium. *Bericht der Römisch-Germanischen Kommission*. 2021;5–82. <https://doi.org/10.11588/bergk.2018.1.85547>.
 37. Kaparou M, Oikonomou A. Mycenaean through Hellenistic glass in Greece: where have we got to? *Archaeol Anthropol Sci*. 2022;14(5):1–5. <https://doi.org/10.1007/s12520-022-01558-7>.
 38. Ignatiadou D. Early Glass in Methone. In: I. Lazar, Editor. *Annales du 19e Congrès de l'Association Internationale pour l'Histoire du Verre Piran 2012*. Koper: 2015;81–88.
 39. Kolesnychenko A, Kiosak D. The Ancient Glass-Workshop of Yahorlyk Settlement in the Northern Pontic Region. In: *Annales du 21e Congrès de l'AIHV Istanbul 2018 O. Sevindik Ed*. Pavia: 2021;81–94.
 40. Koch LC. Die Glasbügelfibeln des 8. und 7. Jahrhunderts aus Etrurien. Ein Beitrag zur eisenzeitlichen Glastechnik und zu den Bestattungssitten des Orientalisante. *Universitätsforschungen zur prähistorischen Archäologie*. Bonn: 2010 190 p.
 41. Koch LC. The large glass beads of leech fibulae from Iron age necropoli in northern Italy. *BEADS*. 2020;32:3–14.
 42. Rehren T, Broschat K. A large turquoise glass writing palette from Tutankhamen's Tomb. *J Glass Stud*. 2020;62:263–6.
 43. Koch LC. Report on the Vitreous Bird Beads (Vogelperlen). *ARIMNESTOS Ricerche di Protostoria Mediterranea* 1/2018. 2018;6(1):225–235.
 44. Savignoni L, Mengarelli R, Caracupa. La necropoli arcaica di Caracupa tra Norba e Sermoneta. *Notizie degli Scavi*. 1903;1903:289–344.
 45. Gierow PG. The Iron Age Culture of Latium. *Excavations and finds*. *Skrifter utgivna av Svenska institutet i Rom*. 1964; 24 Vol.2: 133–430.
 46. Bietti Sestieri AM. La necropoli laziale di Osteria dell'Osa. Roma: Quasar, 1992.
 47. Leonelli V. La necropoli della prima età del ferro delle acciaierie a Terni: contributi per un'edizione critica. *La necropoli della prima età del ferro delle acciaierie a Terni*. Contributi per un'edizione critica Firenze: All'insegna del giglio, 2003, 347p.
 48. Stefani E. Scoperte archeologiche nell'Agro Capenate. *Bollettino di Paletnologia Italiana*. 1912;38:147–58.
 49. Brusadin Laplace D, Patrizi-Montoro G, Patrizi-Montoro S. Le necropoli protostoriche del Sasso di Furbara III. altri sepolcreti villanoviani. *Origini*. 1992;16:221–94.
 50. Brizio E. Verucchio. Scoperta di sepolcreti tipo Villanova. *Notizie degli Scavi*. Roma. 1898:343–90.
 51. Palm J. Veiiian Tomb Groups in the Museo Preistorico. In: *Opuscula Archaeologica*, VII, Acta Instituti Romani Regni Sueciae XVI, Lund, Gleerup 1952; 7 p. 50–86.
 52. Paribeni R. Necropoli del territorio capenate. *Monumenti Antichi dei Lincei*. Roma: Tipografia della Accademia dei Lincei; 1906; 16: 277–490.
 53. Taloni M. Le tombe da Riserva del Truglio al museo Pigorini di Roma. *Officina Etruscologia*, 2013; 437p.
 54. Solé VA, Papillon E, Cotte M, Walter P, Susini J. A multiplatform code for the analysis of energy-dispersive X-ray fluorescence spectra. *Spectrochim Acta, Part B*. 2007;62(1):63–8. <https://doi.org/10.1016/j.sab.2006.12.002>.
 55. Yatsuk O, Ferretti M, Gorghinian A, Fiocco G, Malagodi M, Agostino A, Gulmini M. Data from multiple portable XRF units and their significance for ancient glass studies. *Molecules*. 2022;27(18):6068. <https://doi.org/10.3390/molecules27186068>.
 56. Nolte H, MacVicar TD, Tellkamp F, Krüger M. Instant clue: a software suite for interactive data visualization and analysis. *Sci Rep*. 2018;8(1):1–8. <https://doi.org/10.1038/s41598-018-31154-6>.
 57. Wojdyr M. Fityk: a general-purpose peak fitting program. *J Appl Crystallogr*. 2010;43(5–1):1126–8. <https://doi.org/10.1107/S0021888910030499>.

58. Micheletti F, Orsilli J, Melada J, Gargano M, Ludwig N, Bonizzoni L. The role of IRT in the archaeometric study of ancient glass through XRF and FORS. *Microchem J*. 2020;153:104388. <https://doi.org/10.1016/j.microc.2019.104388>.
59. Aceto M, Fenoglio G, Labate M, Picollo M, Bacci M, Agostino A. A fast non-invasive method for preliminary authentication of mediaeval glass enamels using UV-visible-NIR diffuse reflectance spectrophotometry. *J Cult Herit*. 2020;45:33–40. <https://doi.org/10.1016/j.culher.2020.05.003>.
60. Lahilil S, Biron I, Cotte M, Susini J, Menguy N. Synthesis of calcium antimonate nano-crystals by the 18th dynasty Egyptian glassmakers. *Appl Phys A*. 2010;98(1):1–8. <https://doi.org/10.1007/s00339-009-5454-1>.
61. Gulmini M, Pace M, Ivaldi G, Ponzi MN, Mirti P. Morphological and chemical characterization of weathering products on buried Sasanian glass from central Iraq. *J Non-Cryst Solids*. 2009;355(31–33):1613–21. <https://doi.org/10.1016/j.jnoncrysol.2009.05.056>.
62. Colombari P. Polymerization degree and Raman identification of ancient glasses used for jewelry, ceramic enamels and mosaics. *J Non-Cryst Solids*. 2003;323(1–3):180–7. [https://doi.org/10.1016/S0022-3093\(03\)00303-X](https://doi.org/10.1016/S0022-3093(03)00303-X).
63. Caggiani MC, Mangone A, Mastroiocco F, Taccogna C, Laviano R, Gian-nossa LC. The Tetris game of scientific investigation. Increase the score embedding analytical techniques. Raw materials and production technology of Roman glasses from Pompeii. *Microchem J*. 2017;131:21–30. <https://doi.org/10.1016/j.microc.2016.11.012>.
64. Ricciardi P, Colombari P, Tournié A, Macchiarella M, Ayed N. A non-invasive study of Roman Age mosaic glass tesserae by means of Raman spectroscopy. *J Archaeol Sci*. 2009;36(11):2551–9. <https://doi.org/10.1016/j.jas.2009.07.008>.
65. Tournié A, Prinsloo LC, Colombari P. Raman spectra database of the glass beads excavated on mapungubwe hill and k2, two archaeological sites in South Africa. Preprint: 1012.1465. 2010. <https://doi.org/10.48550/arXiv.1012.1465>.
66. Brems D, Degryse P. Trace elements in sand raw materials. In: Degryse P, editor. *Glass making in the Greco-Roman World. Results of the ARCH-GLASS project*. Leuven: Leuven University Press; 2014. p. 69–85.
67. McLennan SM. Relationships between the trace element composition of sedimentary rocks and upper continental crust. *Geochem Geophys Geosyst*. 2001;20(4):2000GC000109. <https://doi.org/10.1029/2000GC000109>.
68. Gratze B. Provenance analysis of glass artefacts. In: Janssens K, editor. *Modern methods for analysing archaeological and historical glass*. Oxford: John Wiley & Sons; Chichester 2013.
69. Shortland A, Rogers N, Eremin K. Trace element discriminants between Egyptian and Mesopotamian late Bronze age glasses. *J Archaeol Sci*. 2007;34(5):781–9. <https://doi.org/10.1016/j.jas.2006.08.004>.
70. Arletti R, Bertoni E, Vezzalini G, Mengoli D. Glass beads from Villanovian excavations in Bologna (Italy): an archaeometrical investigation. *Eur J Mineral*. 2011;23(6):959–68. <https://doi.org/10.1127/0935-1221/2011/0023-2166>.
71. Reade W. The first thousand years of glass-making in the ancient near east: compositional analyses of late bronze and iron age glasses. *Archaeopress*. 2021. <https://doi.org/10.2307/j.ctv1n9dk03>.
72. Cagno S, Mendera M, Jeffries T, Janssens K. Raw materials for medieval to post-medieval Tuscan glassmaking: new insight from LA-ICP-MS analyses. *J Archaeol Sci*. 2010;37(12):3030–6. <https://doi.org/10.1016/j.jas.2010.06.030>.
73. Aerts A, Velde B, Janssens K, Dijkman W. Change in silica sources in Roman and post-Roman glass. *Spectrochim Acta, Part B*. 2003;58(4):659–67. [https://doi.org/10.1016/S0584-8547\(02\)00287-2](https://doi.org/10.1016/S0584-8547(02)00287-2).
74. Polikreti K, Murphy JMA, Kantarelou V, Karydas AG. XRF analysis of glass beads from the Mycenaean palace of Nestor at Pylos, Peloponnese, Greece: new insight into the LBA glass trade. *J Archaeol Sci*. 2011;38(11):2889–96. <https://doi.org/10.1016/j.jas.2011.05.003>.
75. Schiavon N, Candeias A, Ferreira T, Da Conceição LM, Carneiro A, Calligaro T, Mirao J. A combined multi-analytical approach for the study of Roman glass from south-west Iberia: synchrotron μ -XRF, external-PIXE/PIGE and BSEM-EDS. *Archaeometry*. 2012;54(6):974–96. <https://doi.org/10.1111/j.1475-4754.2012.00662.x>.
76. Henderson J. The raw materials of early glass production. *Oxf J Archaeol*. 1985;4(3):267–91.
77. Rehren T. Rationales in old world base glass compositions. *J Archaeol Sci*. 2000;27(12):1225–34. <https://doi.org/10.1111/j.1468-0092.1985.tb00248.x>.
78. Genga A, Siciliano M, Tepore A, Mangone A, Traini A, Laganara C. An archaeometric approach about the study of medieval glass from Siponto (Foggia, Italy). *Microchem J*. 2008;90(1):56–62. <https://doi.org/10.1016/j.microc.2008.03.008>.
79. Schibille N. Late Byzantine mineral soda high alumina glasses from Asia Minor: a new primary glass production group. *PLoS ONE*. 2011;6(4):e18970. <https://doi.org/10.1371/journal.pone.0018970>.
80. Verità M, Lazzarini L, Tesser E, Antonelli F. Villa del Casale (Piazza Armerina, Sicily): stone and glass tesserae in the baths floor mosaics. *Archaeol Anthropol Sci*. 2019;11(1):373–85. <https://doi.org/10.1007/s12520-017-0559-5>.
81. Henderson J. *Ancient glass: an interdisciplinary exploration*. Cambridge University Press. 2013. <https://doi.org/10.1017/CBO9781139021883>.
82. Towle A, Henderson J. The glass bead game: archaeometric evidence for the existence of an Etruscan glass industry. *Etruscan Studies*. 2004;10(1):47–66. <https://doi.org/10.1515/etst.2004.10.1.47>.
83. Smirniou M, Rehren Th. Shades of blue – cobalt-copper coloured blue glass from New Kingdom Egypt and the Mycenaean world: a matter of production or colourant source? *J Archaeol Sci*. 2013;40(12):4731–43. <https://doi.org/10.1016/j.jas.2013.06.029>.
84. Conte S, Matarese I, Vezzalini G, Pacciarelli M, Scarano T, Vanzetti A, Gratze B, Arletti R. How much is known about glassy materials in Bronze and Iron Age Italy? New data and general overview. *Archaeol Anthropol Sci*. 2019;11(5):1813–41. <https://doi.org/10.1007/s12520-018-0634-6>.
85. Angelini I, Artioli G, Bellintani P, Diella V, Gemmi M, Polla A, Rossi A. Chemical analyses of Bronze Age glasses from Frattesina di Rovigo, northern Italy. *J Archaeol Sci*. 2004;31(8):1175–84. <https://doi.org/10.1016/j.jas.2004.02.015>.
86. Bandiera M, Verità M, Lehuédé P, Vilarigues M. The technology of copper-based red glass Sectilia from the 2nd Century AD Lucius Verus Villa in Rome. *Minerals*. 2020;10(10):875. <https://doi.org/10.3390/min10100875>.
87. Craddock PT. The composition of the copper alloys used by the Greek, Etruscan and Roman civilisations: 2. the Archaic, Classical and Hellenistic Greeks. *J Archaeol Sci*. 1977;4(2):103–23. [https://doi.org/10.1016/0305-4403\(78\)90015-8](https://doi.org/10.1016/0305-4403(78)90015-8).
88. Ingo GM, De Caro T, Riccucci C, Angelini E, Grassini S, Balbi S, Bernardini P, Salvi D, Bousselemi L, Cilingiroglu A, Gener M. Large scale investigation of chemical composition, structure and corrosion mechanism of bronze archaeological artefacts from Mediterranean basin. *Appl Phys A*. 2006;83(4):513–20. <https://doi.org/10.1007/s00339-006-3550-z>.
89. Abe Y, Harimoto R, Kikugawa T, Yazawa K, Nishisaka A, Kawai N, Yoshimura S, Nakai I. Transition in the use of cobalt-blue colorant in the New Kingdom of Egypt. *J Archaeol Sci*. 2012;39(6):1793–808. <https://doi.org/10.1016/j.jas.2012.01.021>.

Publisher's Note

Springer Nature remains neutral with regard to jurisdictional claims in published maps and institutional affiliations.

Submit your manuscript to a SpringerOpen[®] journal and benefit from:

- Convenient online submission
- Rigorous peer review
- Open access: articles freely available online
- High visibility within the field
- Retaining the copyright to your article

Submit your next manuscript at ► [springeropen.com](https://www.springeropen.com)